Doc. Control
LIGO-T960027-01-I

From mike@tristan.mit.edu Fri Apr 19 08:53 PDT 1996
To: betty@tristan.mit.edu
Cc: dhs@tristan.mit.edu
Subject: oops: more copies

Sorry, I guess you need more copies after all; looks like

Gary Sanders
Dennis Coyne
Barry Barish
Robbie Vogt
Fred Raab
Rolf Bork
Bill Althouse
Stan Whitcomb

are supposed to get their own paper copies too. Let me know if there are problems.

Thanks again,

Mike

----- Begin Included Message -----

Betty-

Since David is in transit, he asked me to ask you to distribute a document to the LSC design review panel. This panel consists of

Jay Heefner
Seiji Kawamura
Albert Lazzerini
Jennifer Logan

at Caltech, plus

Peter Fritschel
David Shoemaker
Rai Weiss

at MIT. I have already given the document out to Rai, David and Peter. If you could please print out the file

~mike/T960027/lsc_cdd.fm5.ps (a printer-ready PostScript file)

and distribute it to the Caltech people, I would be most appreciative. They have been forewarned and are expecting it today.

Thanks,

Mike

----- End Included Message -----

LASER INTERFEROMETER GRAVITATIONAL WAVE OBSERVATORY
- LIGO -
CALIFORNIA INSTITUTE OF TECHNOLOGY
MASSACHUSETTS INSTITUTE OF TECHNOLOGY

Document Type	LIGO-T960027-01 -	I	4/18/96

Length Sensing and Control Subsystem Conceptual Design Description

J. Camp, P. Fritschel, L. Sievers and M. Zucker

Distribution of this draft:

LSC DRR Committee

This is an internal working note of the LIGO Project.

California Institute of Technology
LIGO Project - MS 51-33
Pasadena CA 91125
Phone (818) 395-2129
Fax (818) 304-9834
E-mail: info@ligo.caltech.edu

Massachusetts Institute of Technology
LIGO Project - MS 20B-145
Cambridge, MA 01239
Phone (617) 253-4824
Fax (617) 253-7014
E-mail: info@ligo.mit.edu

WWW: http://www.ligo.caltech.edu/

LIGO DRAFT

CONTENTS

LIGO DRAFT

ABSTRACT

We present a conceptual design and supporting analysis for the LIGO Detector Length Sensing and Control subsystem. Principal modes of operation, functions for each mode, and underlying assumptions and dependencies are discussed. A sample control system design for the low-noise Detection mode is presented; its performance is analyzed and compared with established requirements. Focus areas for the preliminary design phase are also highlighted.

Keywords: length sensing, modulation, asymmetry, readout, calibration, acquisition, photodiode, photodetector, topology, shot noise.

1. LSC SUBSYSTEM DESCRIPTION

1.1. Interferometer System Context

The initial LIGO detector system (Figure 1) employs three power-recycled Michelson interferometers with Fabry-Perot cavity arms, each of length 2 km (at Hanford) or 4 km (at Hanford and Livingston). The main Core Optics (CO) components comprising each of these interferometers' optical systems are suspended as pendulums, mounted on seismic isolation stacks (SEI) within the vacuum envelope. They are illuminated by prestabilized laser light (PSL), which is modulated, filtered and modematched to the interferometer by a mode cleaner and other input optics (IOO). Alignment of the core optics to a common optical axis is achieved and maintained by optical lever and wavefront sensors (ASC) acting through suspension actuators (SUS). Light reflected from the core optics is shaped and directed by output optics telescopes and relay mirrors (IOO) to fall on photodetection units, which form the principal input signal interface of the Length Sensing and Control (LSC) system. The LSC provides control loop correction output signals to adjust the distances between core optics (through SUS and SEI) and to tune the laser frequency (through IOO and PSL), and provides the calibrated strain readout to the data acquisition system (CDS DAQ).

1.2. LSC Subsystem Roles

The LSC subsystem is responsible for maintaining optical resonance in the interferometer such that a linear signal, proportional to metric strain, is available at the readout. To accomplish this, LSC must determine and control the four independent length degrees of freedom shown in Figure 2. Each of these lengths must be held to an integral number of half-wavelengths of the laser light ($\lambda = 1.06\ \mu m$) with high accuracy, ranging from 2 nm to less than 1 pm, to achieve the required precision in the strain readout. The readout is derived from the correction signal required to counteract L_-, the difference in the Fabry-Perot arm cavity lengths.

LIGO-T960027-01

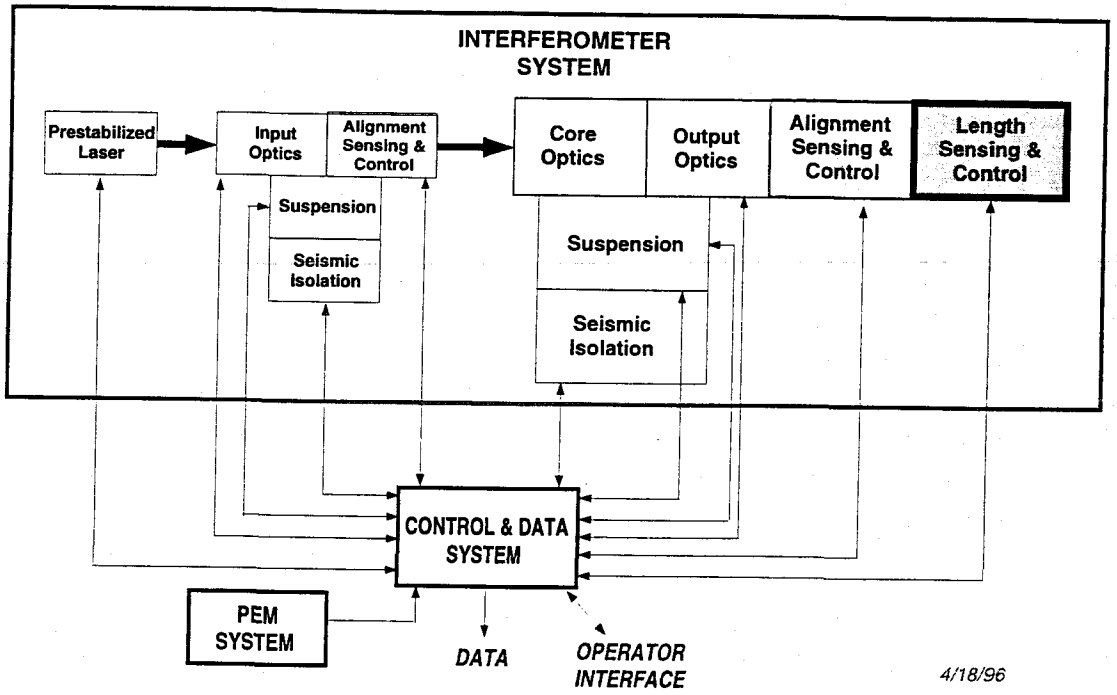

Figure 1: LIGO Detector subsystems (LSC highlighted).

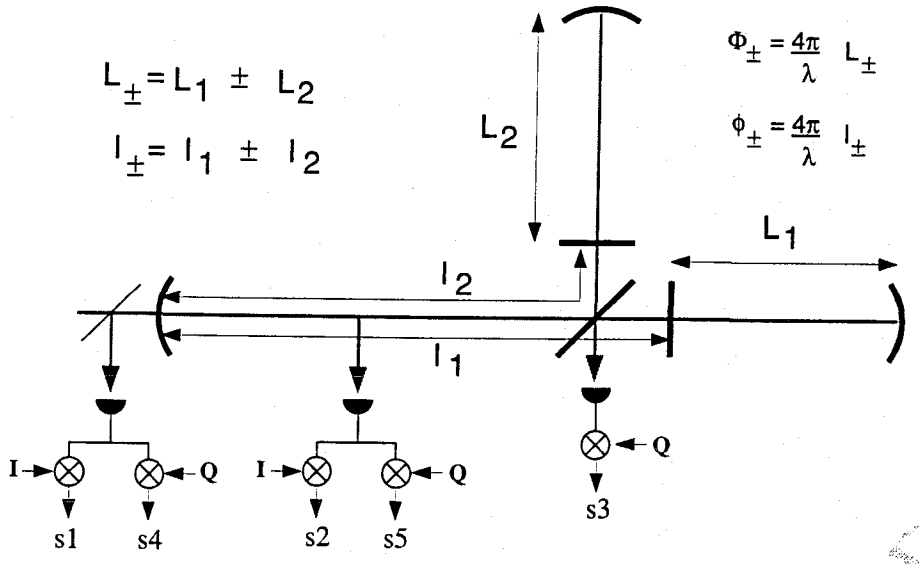

Figure 2: Power recycled interferometer with asymmetry readout: lengths and readout signals.

Functional requirements on the LSC subsystem are detailed in LIGO-T960058-00-I, "LSC Design Requirements." While requirements on accuracy and noise are most stringent for *detection* of gravitational signals, initially or after an interruption the lengths and velocities will be random and incommensurate with the laser wavelength; thus linear signals are not available. LSC must

DRAFT

provide a means for *acquisition* of the linear operating state, wherein dynamic reserve and "intelligent" use of the limited sensor information available to bootstrap toward normal operation are more important than low noise. In addition, LSC must provide *diagnostic and calibration* functions, both for its own operation and commissioning and to support diagnosis of other subsystems. These functions will include operation of reduced optical systems and invasive tests. The requirements for each of these missions are different and (in some cases) conflicting, so it is necessary to define subsets of LSC functionality in terms of distinct modes of operation.

1.3. Modes of LSC Operation

1.3.1. Acquisition

At startup or after an interruption the six[1] core optics will be under local SUS control, with random motions averaging several microns in amplitude. After the Alignment Sensing and Control (ASC) subsystem achieves adequate alignment to enable optical resonance, the LSC will be engaged in Acquisition mode. In this mode LSC will interpret the superposition of complex, nonlinear transients generated as each pair of mirrors passes briefly through resonance, slow the mirrors if needed, and sequence a series of robust control loops to achieve simultaneous resonance in all cavities. This control mode is characterized by the need for high dynamic range, precise sequence triggering and timing, and possibly nonlinear predictive signal processing; signal-to-noise ratio is a secondary issue.

1.3.2. Transition

After acquisition, a settling period is required. Control loops capable of maintaining the tight control and low noise level appropriate for signal detection will have compromised dynamic reserve and narrow operating margins, making them vulnerable to overload from residual transient excitations or alignment variations. Wire and mirror resonances are permitted to settle down (or are actively damped), filters allowed to equilibrate, and self-tests are completed to verify that residual excitations do not exceed Detection mode limits. After cavities are in resonance and the circulating fields equilibrated, the ASC subsystem is permitted to advance to its Detection mode (wherein alignment signals are derived from the wavefront sensors). Alignment adjustments are then permitted to converge and settle.

1.3.3. Detection

The Detection mode is essentially the normal operating state of the interferometer, in which the strain readout is provided at the design noise level. This performance target, and the minimum fraction of time the interferometer may be in this mode, descend directly from the Science Requirements Document LIGO-E950018-00-E.

Control loop gains for each degree of freedom affect the readout noise through a number of effects. The design must strike a balance between competing noise effects and implementation constraints, such as dynamic range limits, mechanical resonances, and propagation delays (see Section 3.).

1. eight, for the Washington 2 km interferometer

The strain signal readout (and possibly other monitored signals, TBD) must have a traceable and accurate absolute calibration throughout the measurement frequency band (40 Hz to 10 kHz) available at all times in Detection mode. Aside from initial calibration errors, there will be fluctuations in the effective transfer function from strain to readout voltage due to changes in modulation source output, tuning, photodiode quantum efficiency, laser output, optical alignment, etc. These may necessitate continuous end-to-end calibration, as well as periodic frequency response calibration measurements (see Section 6. below).

In addition to calibrating the readout signal, it will be necessary to filter it to suit the dynamic range of the digital recording system. Significant spectral whitening is required to represent the strain signal digitally within CDS DAQ word length and sample rate constraints. This function is provided by the LSC readout. Although this filtering will not be trivial, the causal delay constraints which limit realtime servo filter transfer functions do not apply to the readout.

1.3.4. Diagnostic and Calibration

This operating "mode" actually includes an expandable set of modes, loosely defined by the common properties that:

- special degrees of freedom or parameters are enhanced to enable separability and characterization
- the interferometer is not required to provide astrophysical data at the design sensitivity.

Diagnostic mode categories currently under consideration are described below, in order of increasing degree of invasiveness (and, inversely, by their expected frequency of application).

1.3.4.1 Stimulus-response diagnostics

Stimulus-response diagnostic testing must be available for all control states (i.e. transition to this diagnostic mode must be directly accessible from Acquisition, Transition and Detection operating modes, as well as from other Diagnostic modes). In this mode a test signal (generated by CDS Remote Diagnostics equipment/software) is directed to an injection test point or points, and system outputs are monitored (by a combination of CDS Remote Diagnostics and Data Acquisition equipment/software) to determine the transfer function and other characteristics. The amount of test signal power required for accurate measurements, and the presence of the additional waveform source and readout connections, will generally limit the usefulness of strain data recorded during these tests.

One example, expected to arise frequently, is a swept sine calibration to determine the overall frequency response between gravitational wave strain and LSC readout voltage (see Section 6.). Sinusoidal test signals at successive frequencies are applied to a summing node in the L loop to apply forces to the test masses, simulating the effect of gravitational waves; the response magnitude and phase are recorded, and normalized by the known electromechanical coefficients of the electronics and actuators. Other tests in this category involve simultaneously adding an offset or out-of-band signal to another test point, to determine parametric sensitivities (e.g. to laser intensity noise).

Most other interferometer subsystems and the interferometer as a whole will also be subjected to stimulus-response tests. LSC-supported readout of test signals injected throughout the interferometer will be a principal means to gauge other subsystems' performance and interactions. Tests in this category are discussed further in LIGO-T960031-00-E, "CDS Online Diagnostic and Readout Functions."

1.3.4.2 Variations in control topology

To isolate control path interactions and noise sources it will be necessary to disable or disturb one or more feedback paths while leaving other paths operational. For example, the common-mode L_+ loop could be operated with feedback to the SEI/SUS actuators disabled or attenuated, or with feedback to the PSL disabled or attenuated. Each of these conditions would temporarily compromise sensitivity, but would enable effective separation of laser frequency, seismic and electronic noise effects, as well as permit effective characterization of the "disabled" feedback path's transfer function. However, reallocation of loop gain or dynamic range may be necessary to accomplish this. Such diagnostic control variants will be considered throughout the controls design process; where feasible, Acquisition and Detection mode control solutions which provide these capabilities naturally will be favored. Other examples of diagnostics involving control topology variation may include:

- removal of DM (or CM) length control signals from ITM (or ETM) drive paths
- disabling SEI drift/tidal motion feedback for one or more optics
- radical alteration of L_- loop gain (to probe relationship between auxiliary sensor shot noise, residual fringe error, and intensity noise, for example; see 3.1.).

1.3.4.3 Variations in optical topology

To successfully commission the LIGO detector, verify operation of its component subsystems, and determine its parameters for subsequent optimization, it is necessary to operate subsets of its optical system. LSC controls will support the following "reduced" interferometer optical configurations:

- recycled singlebounce Michelson interferometer (ETM's blocked or grossly misaligned).
- simple Michelson interferometer (RM removed, ETM's blocked or grossly misaligned)
- coupled cavity (BS removed, or high reflector substituted)
- unrecycled FP michelson (RM removed)
- single, uncoupled Fabry-Perot cavity (RM removed, one cavity blocked or misaligned)

With the possible exception of the first (recycled Michelson), each of these involves radical alteration of the in-vacuum optics, so use of these modes after commissioning is expected to be infrequent. The design optimization will favor solutions which provide these capabilities automatically as subsets of the normal control modes, to minimize the additional investment of dedicated hardware and software in these applications. This depends on early delineation of the commissioning sequence.

1.4. Conceptual Design Overview

Where possible, we have tried to indicate how the design presented below is responsive to the requirements set forth in LIGO-T960058-00-I, "LSC Design Requirements Document." In many cases there are significant design variations and options available and under active consideration; some are discussed briefly in Appendix D and referenced documents. Design analysis is in its early stages, and prototype testing has not yet begun, so significant revisions are possible; this document will be updated or superseded to reflect such changes, as necessary.

Figure 3 shows the conceptual design broken into its functional subunits; these are defined and described later in this document. The principal signal and control interfaces with other detector subsystems are also shown here. Some of these interfaces have special characteristics, which we highlight next.

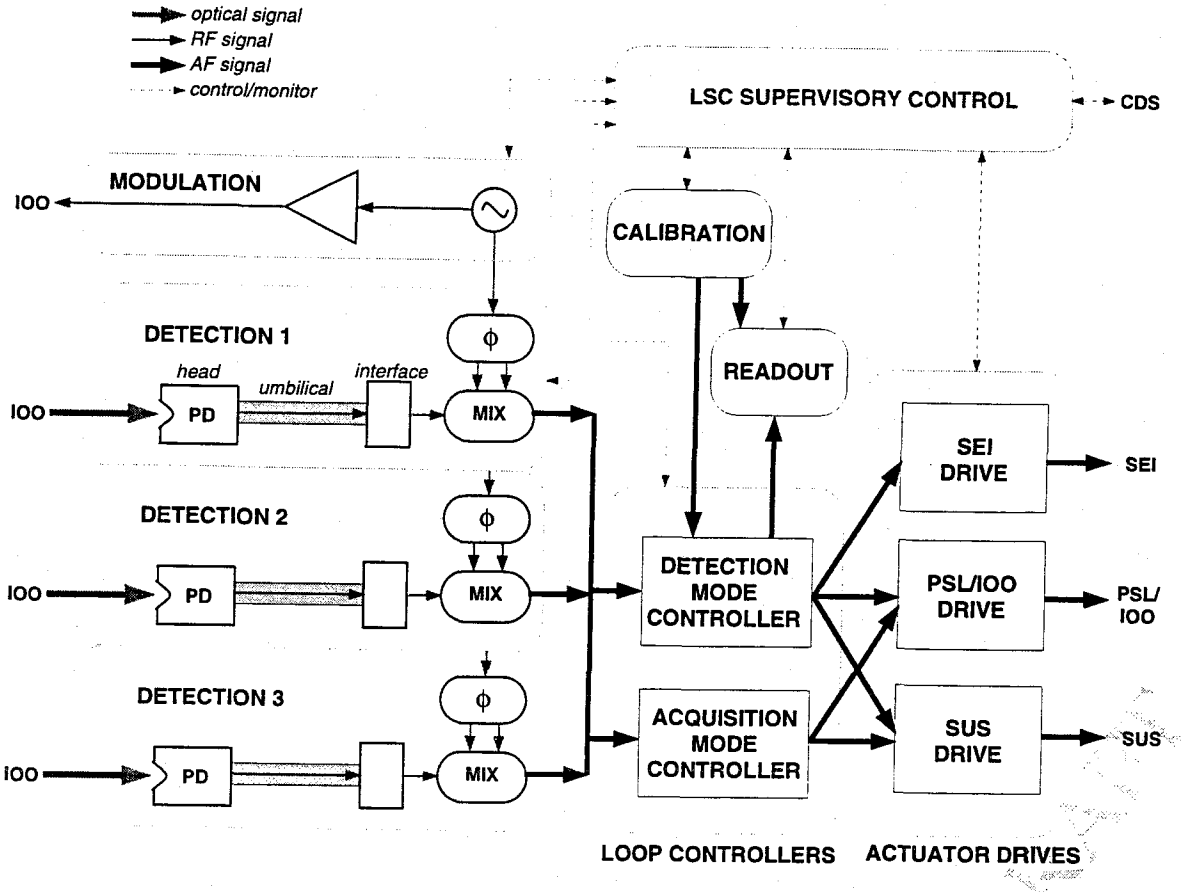

Figure 3: LSC subsystem functional block diagram, showing principal signal interfaces.

1.4.1. Closely related interferometer subsystems

The length sensing and control functions depend on successful operation of all other detector subsystems. LSC's special role in system-level detector diagnostics is a direct consequence of this

hierarchical dependence. In addition, certain direct functional interdependencies with other subsystems strongly impact LSC design strategy and implementation.

1.4.1.1 Input/Output Optics and Prestabilized Laser

The prestabilized laser/input optics mode cleaner combination is expected to deliver light with a fractional frequency stability no better than $4x10^{-18}$ $Hz^{-1/2}$ at 100 Hz. A possible 1% mismatch in the storage time or loss of the arm cavities would translate this into an apparent strain noise of $4x10^{-20}$ $Hz^{-1/2}$, exceeding the SRD noise goal by a factor of 2000. As a result, high-gain wideband feedback is required from the common-mode L+ loop to reduce the residual laser fractional frequency fluctuation to the level of 3 10^{-22} $Hz^{-1/2}$ near 100 Hz. To effect this correction, LSC will pass a filtered, wideband signal derived from demodulator output **s1** (Figure 2) back to the IOO and PSL.

The close coupling between LSC and IOO/PSL control loops requires a large degree of design coordination. LSC loop characteristics will depend critically on the transfer function provided by IOO/PSL, which in turn depends on the IOO/PSL stabilization loop gains, operating conditions (e.g., power on internal photodetectors, modulation index, and cavity visibilities), and reference cavity and mode cleaner storage time. Also, although the transmission of the IOO mode cleaner will be normalized by PSL intensity stabilization, variation in the mode cleaner storage time will alter the transfer function from LSC correction signal to laser phase. The LSC loop's tolerance to variations in each of these parameters is small; the demand for high frequency noise suppression conspires with cavity bandwidth limits to sharply constrain LSC gain and phase margins (see Section 3.).

Dynamic range of the IOO/PSL servo will also be critical, especially during LSC acquisition. Prototype experience suggests that laser loop designs which appear robust in normal "standalone" operation do not necessarily survive this test. An adequate signal-to-noise ratio commensurate with the final frequency noise budget must also be preserved through the IOO/PSL loop extension. Finally, the LSC-generated RF modulation voltage must interface with an IOO electrooptic cell to provide pure phase modulation of the requisite index, with a minimum of residual amplitude and polarization modulation and tolerable thermal distortion.

1.4.1.2 Seismic Isolation and Suspension

LSC will also feed signals to the core optics suspensions and seismic isolation stacks to actuate length control. The transfer function, noise, dynamic range, filtering and other characteristics of these signal paths factor into the design of the LSC loop controllers. Initial accuracy and stability of the transfer function over temperature and time will also figure in the LSC calibration budget. Dynamic range of both SUS and SEI actuators will largely affect the availability of the interferometer and times required for lock acquisition and transition.

Sequencing and state transitions in the SUS and SEI subsystems will be governed by LSC signals. During Acquisition local test mass damping will be active, but for noise reasons the local damping must be disabled before transition to Detection mode. Conversely, after loss of lock, local damping is reinstated immediately to reduce transient motion. On loss of lock SEI actuators may be signaled by LSC to hold their last settings, execute a scan, or return to midrange.

1.4.1.3 Control and Data System

LSC is peculiar among detector subsystems in that its WBS description contains no actual hardware (or software, for that matter). All LSC implementation is provided by Control and Data System (CDS) personnel and materials. This is a reflection of the subsystem's nature; LSC functions are all electronic. One symptom is an unusual coupling with CDS, such that an LSC/CDS "interface" appears to defy definition. As a result we suppress the formal boundary between "IFO LSC" and "CDS LSC" throughout this document, and consider the design as an integrated effort.

1.4.1.4 Alignment Sensing and Control

Length sensing acquisition depends on alignment being within ~ a few 10^{-7} radians of ideal for all optics; readout at the design noise level requires 10^{-8} radians or less (see LIGO-T952007-00-I, "ASC Design Requirements Document"). However, ASC achievement of this higher resolution (the ASC "Detection" mode) requires wavefront sensing to be active, and this in turn requires resonance in all cavities. This chicken-egg problem leads to the alternation of state transitions depicted in Figure 4. The inter-subsystem signaling is best handled at the supervisory control level, although availability and transition time requirements may force a lower-level "hardware" sequence logic to be adopted for speed.

ASC uses samples of the same interferometer output beams used for LSC, and the space near the chamber beam I/O ports will be shared between LSC detector heads and ASC wavefront sensor heads. Since the ASC reserved space requirements are expected to be larger (even though most of the beam power goes to LSC detector heads) the detector support platforms are carried under the ASC scope of work.

ASC also requires LSC to provide modulation sidebands suitable for wavefront sensing operation. In the current design concept for both subsystems, this has no serious impact; modulation frequency and depth adequate for LSC needs is also considered adequate for ASC functions. The dependence is nonetheless noted in case designs evolve otherwise.

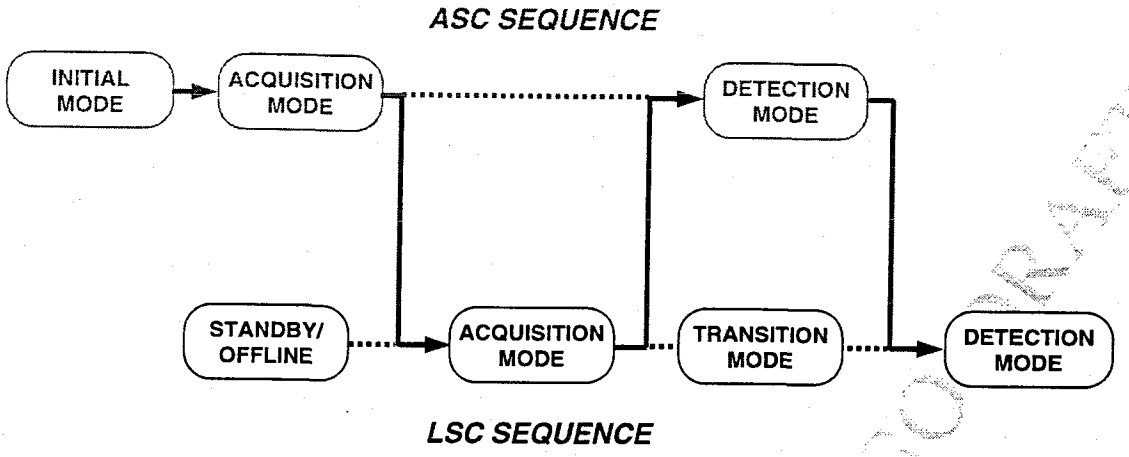

Figure 4: LSC and ASC state transitions during lock acquisition

1.4.2. Equipment Locations and Inter-Station Signal Transmission

IOO relay optics will provide optical beams to LSC photodetectors mounted near the vacuum envelope (_outside_ the vacuum envelope) in the corner station LVEA. The beam providing signals **s2** and **s5** is derived from the wedge reflection off the ITM. Approximate locations of this and the other outputs are shown in Figure 5; Table 1 shows which signals originate in each location.

Each photodetector is supplied with power and control instructions and transmits its signals via an umbilical back to the nearest CDS equipment rack in the LVEA. Most of the LSC control loop functions are implemented here. Actuation and state signals generated for CDS, IOO, SUS and SEI actuators, and data readouts for CDS DAQ and control functions are passed to the corresponding controllers by coaxial cable or network data link within the corner station.

LSC signals passed to end station SEI and SUS actuators may need to be treated differently because coaxial cables are not available between station buildings in the LIGO facilities. Practical limitations on the bandwidth and dynamic reserve of CDS data links provided between LIGO stations will probably demand special hardware and/or software to encode the precision length control signals without adding unacceptable noise artifacts. Implementation of these links is a significant area of concern, and will be a high priority of the preliminary design.

This picture is under construction.

Figure 5: LSC equipment locations in corner station LVEA (Livingston site shown).

Signals	*LA*	*WA 4k*	*WA 2k*
s1, s4	LHAM-2	WHAM-2	WHAM-8
s2, s5	LHAM-5	WHAM-5	WHAM-11
s3	LHAM-6	WHAM-6	WHAM-12

Table 1: LSC photodetector locations by Vacuum Equipment chamber designation (preliminary; see PSI V049-5-001 or equivalent for chamber designation key.)

LIGO-T960027-01

2. READOUT TOPOLOGY & MODULATION

An asymmetry readout scheme is used, as described in LIGO-P940002-00-I. Referring to Figure 2, a sinusoidal radiofrequency modulation signal at $f_m \approx 40$ MHz is applied to an electrooptic modulator (which is itself part of the IOO subsystem) to impose phase modulation on the carrier laser beam. A modulation index of approximately 0.5 is required (precise choice depending on exact mirror parameters, TBD; see LIGO-T960058-00-I). Upper and lower sidebands are both resonant with the average length of the recycling cavity (l_1+l_2), but nonresonant in the Fabry-Perot arm cavities. An asymmetry has been introduced by placing one Fabry-Perot cavity 20-50 cm farther from the beamsplitter than the other; this causes the sideband field traveling to the upper cavity and back to return partly out of phase with that traveling toward the right, and their destructive interference is imperfect. The sideband field thus appears at the "antisymmetric" or "dark" port and falls on the photodetector.

The carrier beam is resonant in both Fabry-Perot arm cavities; since these cavities are overcoupled (the input coupler transmission exceeds the sum of all losses in each cavity) the reflected carrier light is inverted in phase. With this unusual boundary condition, the carrier is made simultaneously resonant in the recycling cavity by choosing its mean length to be midway between two integral half wavelengths. The simultaneous resonance permits power buildup (recycling) by a factor of about 30 inside the recycling cavity.

The modulation signal is provided to the IOO electrooptic modulator[1] by a precision, low-noise oscillator. The fractional SSB amplitude and phase noise of this oscillator must be especially low; an evaluation of the mechanisms leading to this and other RF source specifications may be found in LIGO-T960019-00-D. An additional concern is the degree to which the electrooptic modulator induces residual amplitude modulation (as opposed to pure phase modulation) in the laser light; such AM would induce a static fringe offset in the length control servos, contributing to the RMS deviation from perfect resonance (see Section 3. below). RF pickup and poor circuit isolation can contribute similar offset errors.

1. If the modulator supplied by IOO is not intrinsically matched to the LSC RF generator, LSC will also provide the appropriate LC matching network and connectors.

3. DETECTION MODE CONTROLS

Principal parameters affecting the LSC detection mode controls design are listed in Table 1. Note that many of these are still TBD; likely choices for these (listed in the right-hand column) have been used to complete a sample servo design and closed loop noise propagation study. The results, described below, give confidence that a control design fulfilling LSC detection mode requirements exists within reasonable parameter constraints, and also demonstrate the necessary methods and modeling tools for further optimization in the preliminary design phase.

Table 2: Interferometer parameters assumed in sample Detection mode servo design and noise studies.

Parameter	*Value*
Arm cavity length	4000.0002808 m
Arm input mirror transmission	0.03
Mirror loss (each optic)	50 ppm
Arm end mirror transmission	0 ppm
Average recycling cavity length	5.9970018 m
Recycling mirror transmission	0.0333
Beamsplitter reflectivity	0.49995
Asymmetry (add to one arm, subtract from other)	12.9 cm
Modulation frequency 1	37.4928 MHz
Modulation index	0.476
Carrier wavelength	1.06 microns
Input power	5 watts

Section 3.1. lists the specific requirements and gives references to where they were derived. The servo configuration, including a discussion of alternate variants, is included in Section 3.2., and Section 3.3. describes the sample servo design and gives an evaluation of its closed loop performance.

3.1. Servo Requirements

Servo requirements were initially estimated in Appendix B of Martin Regehr's thesis, LIGO-P940002-00-I. They have been refined and updated in the LSC DRD, LIGO-T960058-00-I, and supporting documents. The requirements relevant to the servo design are summarized below:

1. Arm cavity differential mode loop (driven by intensity noise specification)
   - $|L_1-L_2| < 10^{-12}\ m_{rms}$
   - Loop gain < 10^{-7} at 8 kHz (first test mass resonance)
   - Shot noise contributed by this loop must be at or below the LIGO SRD initial interferometer strain sensitivity requirement at all frequencies
2. Michelson differential mode loop (driven by intensity noise specification)
   - $|l_1-l_2| < 1.3\text{x}10^{-10}\ m_{rms}$
   - Loop gain < 10^{-7} at 8 kHz (first test mass resonance)
   - Shot noise contributed by this loop must be at least a factor of 10 below the SRD sensitivity requirement (which is equal to L_1-L_2 loop shot noise at frequencies above 150 Hz).
3. Arm cavity common mode loop (driven by specification for power in arm cavity)
   - $|L_1+L_2| < 4\text{x}10^{-12}\ m_{rms}$
   - Loop gain < 10^{-7} at 8 kHz (first test mass resonance)
   - Gain must exceed l_1+l_2 loop gain by at least a factor of 130 (preferably more)
   - Shot noise contributed by this loop must be at least a factor of 10 below the SRD sensitivity requirement (which is equal to L_1-L_2 loop shot noise at frequencies above 150 Hz).
4. Michelson common mode loop (driven by specification for power in Recycling cavity)
   - $|l_1+l_2| < 5\text{x}10^{-10}\ m_{rms}$
   - Loop gain < 10^{-7} at 8 kHz (first test mass resonance)
   - Shot noise contributed by this loop must be at least a factor of 10 below the SRD sensitivity requirement (which is equal to L_1-L_2 loop shot noise at frequencies above 150 Hz).

3.2. Servo Configuration

There are a number of servo configurations possible for LIGO. As currently specified, local suspension damping sensors would introduce unacceptable displacement noise if their signals were applied to test masses in Detection mode. However, this level of displacement noise is tolerable for the beam splitter, folding mirrors and recycling mirror since the L_1-L_2 signal is less sensitive to their positions; thus the baseline actuation scheme is for SUS to damp the recycling mirror and the beam splitter locally, while LSC provides interferometric control to the test masses. The noise levels of the local suspension damping sensors are discussed in the Suspension DRD, LIGO-T950011-06-D.

The signals to be sensed for controlling the laser frequency/phase, the arm cavity common mode motion and arm cavity differential mode motion have been specified; they are the in-phase component of the light returning towards the laser (i.e. i_1 in Figure 6) and the quadrature-phase beam splitter anti-symmetric port component (i.e. i_3 in Figure 6), respectively. Several signal choices are available for controlling the Michelson degrees of freedom; these will be definitized in the preliminary design phase.

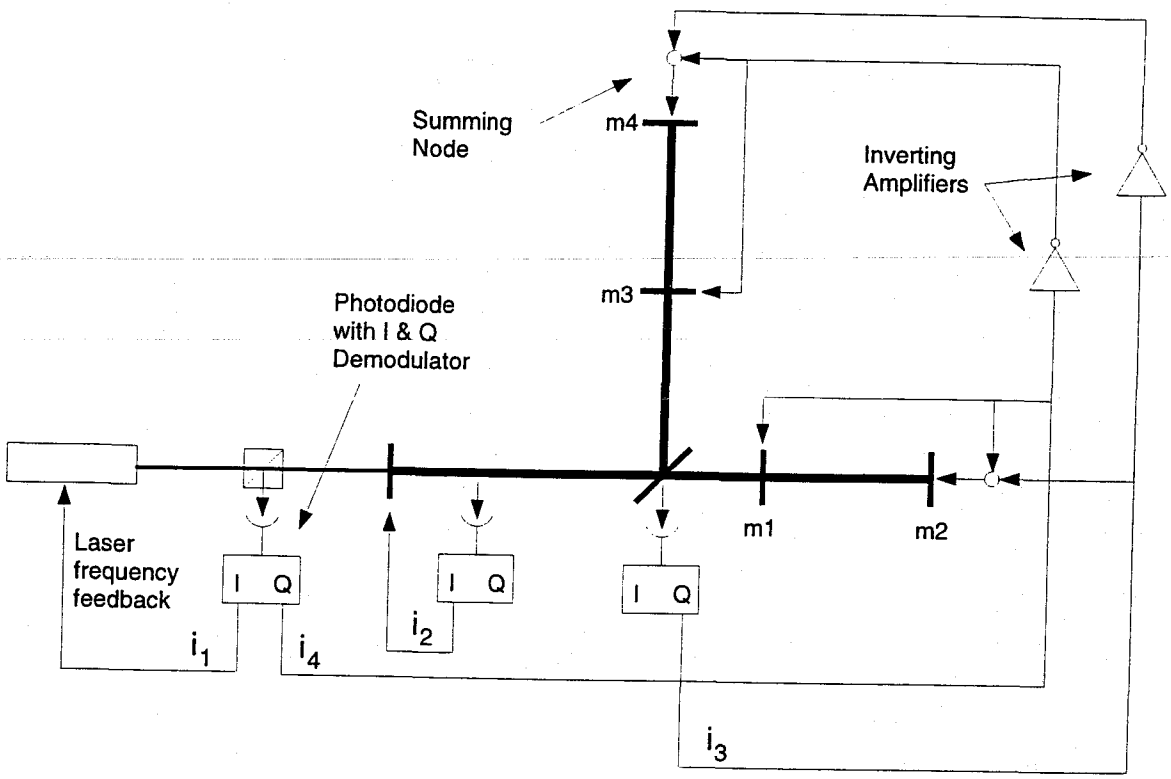

Figure 6: Feedback configuration for sample design analysis

The servo feedback configuration chosen for this analysis is shown in Figure 6. For the control bandwidths under consideration, the following changes to the servo configuration do not affect the servo design or analysis in any significant way (assuming the parameter set in Table 2):

1. i_2: feedback to (m1+m2)+(m3+m4) is equivalent to feedback to the recycling mirror
2. i_4: feedback to (m1+m2)-(m3+m4) is equivalent to feedback to the beam splitter.

This configuration differs from the intended LIGO topology in that the i_2 common-mode feedback is applied to the recycling mirror, rather than to the cavity mirrors. However, since condition (1) above holds for the chosen parameter set, the salient features of the design are equivalent.

For LIGO, it will also be necessary to feed a heavily filtered sample of the i_1 signal to (m2+m4) in order to control the arm cavity common mode motion at low frequencies. This permits the laser wavelength to follow the PSL reference cavity length over long timescales, rather than tracking the common mode arm cavity length. The reference cavity may provide a more stable length reference at low frequencies (< 10 Hz), potentially demanding less range from the laser frequency actuation and reducing the absolute wavelength fluctuation (a possible concern for scattered light noise). This feedback path was not included, as it does not impact any of the direct effects mod-

eled here. However, if not absolutely symmetrical, this feedback path can compromise the common-mode rejection ratio isolating the strain readout from laser frequency noise, so proper balancing and effective filtering are critical design considerations.

A further simplifying omission from the model servo configuration is a feedback path to the stack actuators. This path is necessary in order to get the range needed over a 24 hour period for the arm cavity length fluctuations. The range of the test mass magnet/coils will compensate for the microseismic peak (see LIGO-T950011-06-D) but is not designed to handle the tidal forces or facility drifts. Its inclusion would not affect the analysis, since the bandwidth is well separated from the critical noise and gain constraint regions (crossover frequency would be about 3 mHz).

Another topology variation has been proposed that would make the l_1-l_2 loop more robust to changes in the losses of the cavity mirrors, although the sensitivity in this loop would be decreased somewhat. Signal i_4 depends critically on how well the recycling mirror transmission matches the total losses in the interferometer, a condition that may well change with alignment, contamination or other factors. The Q phase of the recycling cavity circulating field sample (signal s_5 in Figure 2) carries similar information to i_4 and is relatively insensitive to matching conditions, although its shot noise is higher in equivalent terms.

Finally, it has recently been shown that the Alignment Sensing and Control (ASC) wavefront sensing system may require a second modulation at a nonresonant frequency, to allow nondegenerate decomposition of the recycling mirror angle from the common-mode cavity input coupler angle. If this added modulation is present it may be advantageous to derive LSC information from it as well. For example, the signal used for controlling l_1-l_2 could be obtained by demodulating the light returning towards the laser with the second nonresonant modulation; see Appendix D.2. The restrictive l_1-l_2 loop gain constraint could be significantly relaxed in this case. This idea will receive further study in the preliminary design phase.

3.3. Sample Servo Design and Performance Evaluation

Regehr discovered that when high gain laser frequency correction is applied, the plant transfer function matrix is essentially diagonalized. The remaining loops can then be designed assuming that they are uncoupled from the rest of the system. In general, this was the design approach we also chose to pursue. Each of the loops is conditionally stable since it is necessary to maximize low frequency gain but minimize bandwidth in order to meet performance and stability requirements.

Figures 7 through 10 show the chosen loop gains in each of the loops, and Table 3 summarizes the performance of the servo system for each degree of freedom. Plant and controller transfer functions are plotted individually in LIGO-T960032-03-I, "Concept for LSC Design During Detection Mode" by L. Sievers.

The sample design achieves most of the performance goals discussed in 3.1. with some margin, but additional optimization is still necessary. In particular, the open-loop gain in the L_1-L_2 loop exceeds the target by a factor of about 100 at 8 kHz, the residual l_1-l_2 motion is about 15% too high, and the shot noise contribution from the l_1-l_2 sensor is a factor of 1.6 too high. The latter two problems are addressed below. We believe the 8 kHz gain exceedance can be eliminated by applying notch filters at the specific resonance frequencies of the test mass internal modes or by using a more aggressive lowpass filter design above the unity-gain frequency. Both techniques have been successfully applied on the 40 meter and PNI prototype interferometers.

Table 3: Performance of sample servo design. Departures from requirements of Section 3.1. are shown shaded; see text for discussion.

Parameter/result	*L_1+L_2 /Laser Frequency loop*	*l_1+l_2 loop*	*L_1-L_2 loop*	*l_1-l_2 loop*
Gain @ 1 Hz	10^6	3×10^3	3×10^6	2×10^3
Unity-gain (Hz)	10^4	55	140	22
Phase margin	45°	46°	36°	40°
Gain margin	8	3	4	7
Gain @ 8 kHz	~1	2×10^{-8}	10^{-5}	10^{-8}
Plant transfer function fit poles and zeros (Hz)	p=[1.2, 50k] z=[.01, 9.4k]	p=[1.3] z=[.51]	p=[91] z=[19k]	p=[100k] z=[]
Controller poles and zeros (Hz)	p=[50, 50, 100, 100, 10k, 30k] z=[1k, 1k, 2k]	p=[.1, .1, 100, 300, 300, 800, 800, 1k, -.74j, .74j] z=[.74, .74, 40, 40]	p=[.1, .1, 500, 1k, 1k, -.74j, 74j] z=[10, 40, 40, 50]	p=[.1, .1, 80, 500, 500, 500, .74j, -.74j] z=[1, 5, 5]
Closed loop residual RMS motion	N/A[a]	$1.2\times10^{-11}m_{rms}$	$1.15\times10^{-13}m_{rms}$	$1.5\times10^{-10}m_{rms}$

a. As modeled, the common-mode feedback loop did not apply displacement correction to the arm cavities (see text); however, the equivalent error *with respect to the laser wavelength* is 8×10^{-13} meters RMS.

LIGO-T

Figure 7: Loop Gain for Laser (L_+) Loop.

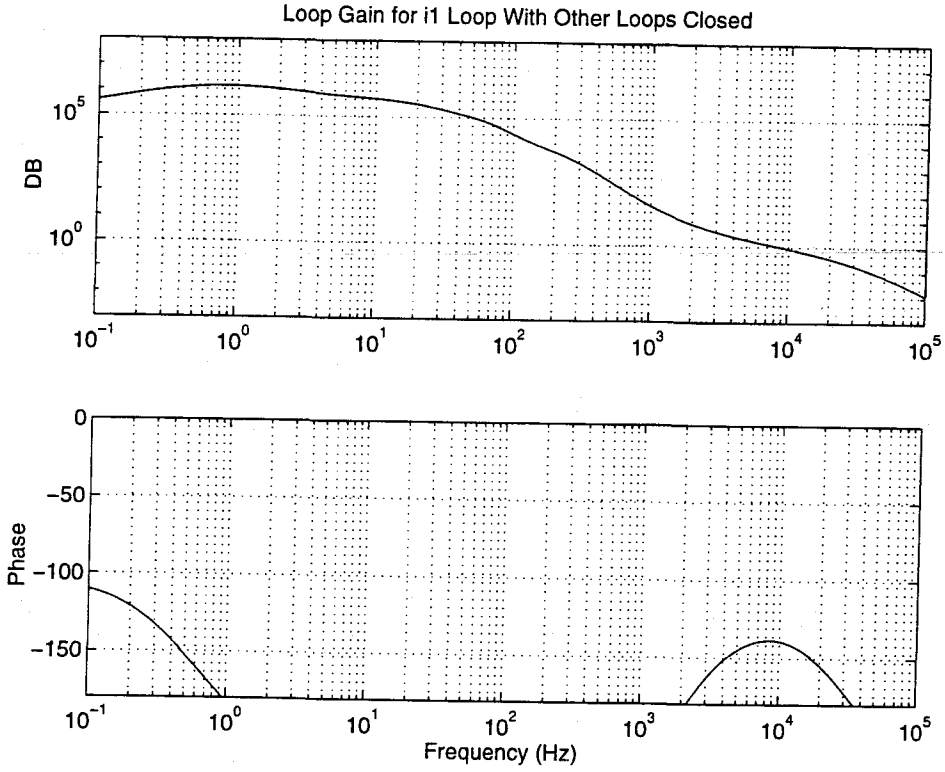

Figure 8: Loop Gain for l_+ Loop.

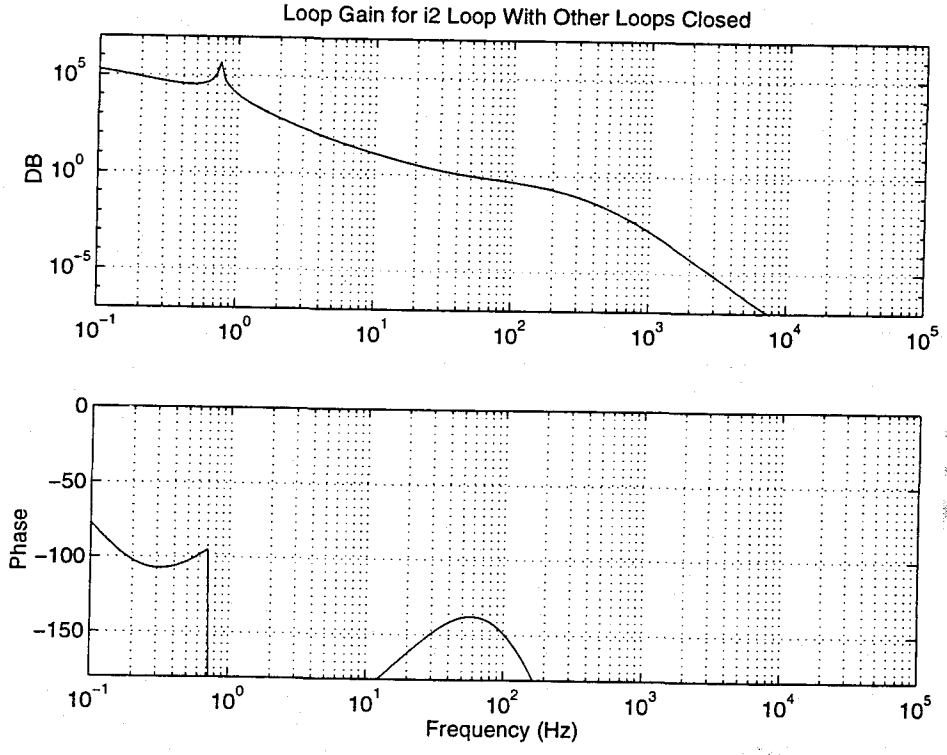

Figure 9: Loop Gain for L_ Loop.

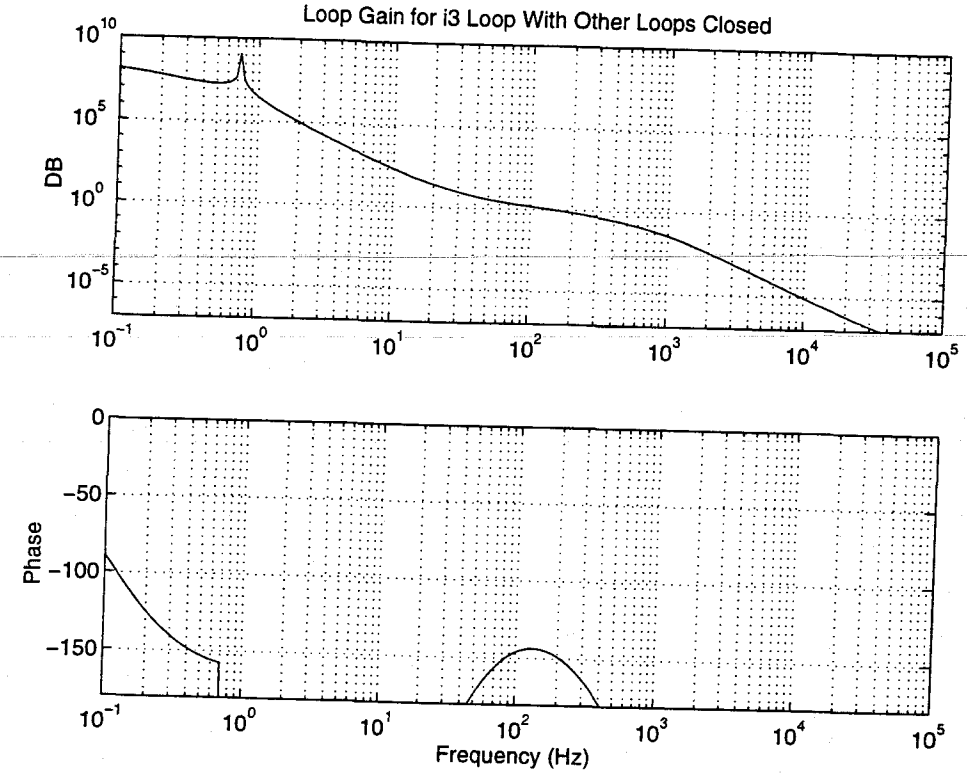

Figure 10: Loop Gain for l_ Loop.

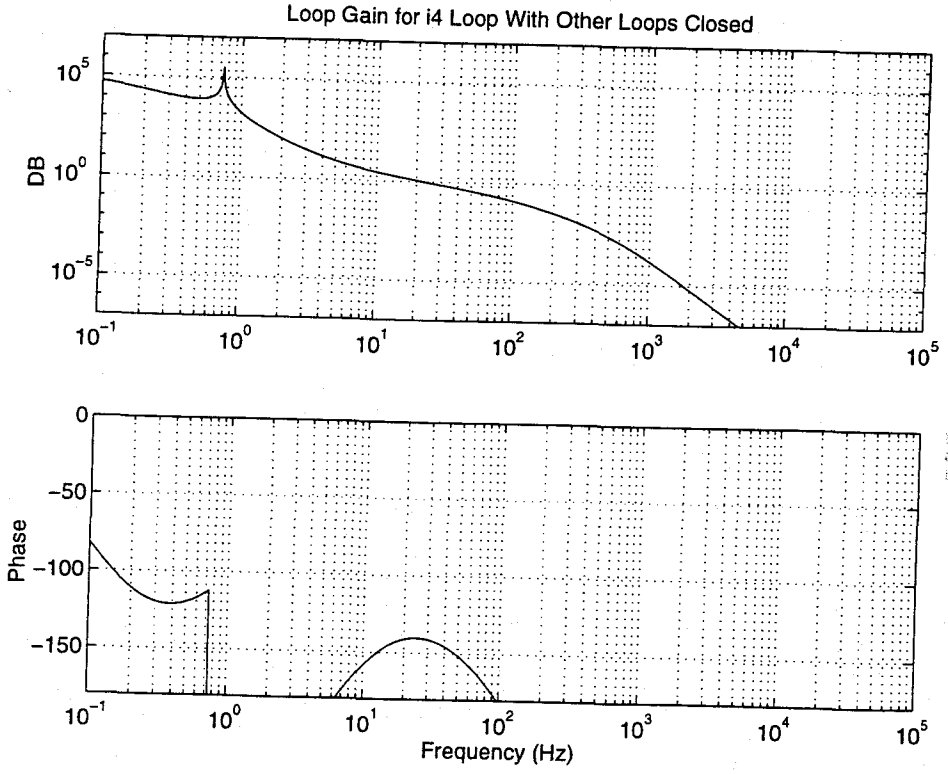

3.3.1. Results: Residual RMS Motion

To calculate the closed loop residual motion for each degree of freedom it was necessary to make assumptions about the seismic input noise and the isolation stack and suspension transfer functions. These assumptions are listed in Appendix A, and result in an open loop motion of 10^{-6} m_{rms} for each test mass. Uncorrelated motions of the same magnitude were assigned to each test mass; as we will see, this may be a significant oversimplification. Figures 11 through 13 show the power spectral density of the closed loop residual motion for each of the loops and list the resulting RMS values.

Figure 14 shows cumulative RMS motion as a function of frequency for the l_1-l_2 loop; briefly, this represents the square root of the definite integral of the residual motion power spectrum from DC up to frequency *f*. This depiction clearly shows that, whether the loop is closed or open, the RMS motion is dominated by the microseismic peak at 0.16 Hz. The l_1+l_2 and L_1-L_2 cumulative RMS plots have the same behavior.

The chosen servo design meets all but one of the closed-loop residual motion requirements. Under the assumed seismic input, the l_1-l_2 residual of $1.5\text{x}10^{-10}$ m_{rms} slightly exceeds the imposed limit of $1.3\text{x}10^{-10}$ m_{rms}. However, the seismic input assumed is believed to be extremely conservative (see Section 3.3.2. below). This gives us confidence that the current design will actually be shown to comply with the residual motion requirement (with significant margin) when a more realistic microseismic excitation model is used.

LIGO-T960027-01

Figure 11: Open and Closed Loop RMS Motion for l_+ Loop.

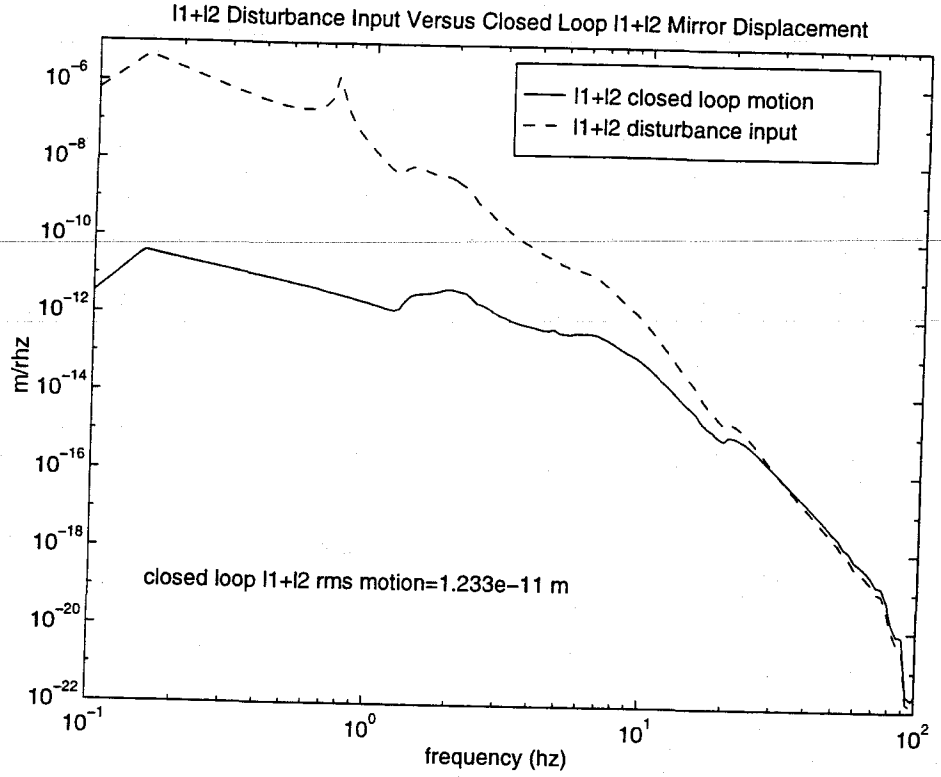

Figure 12: Open and Closed Loop RMS Motion for L_- Loop.

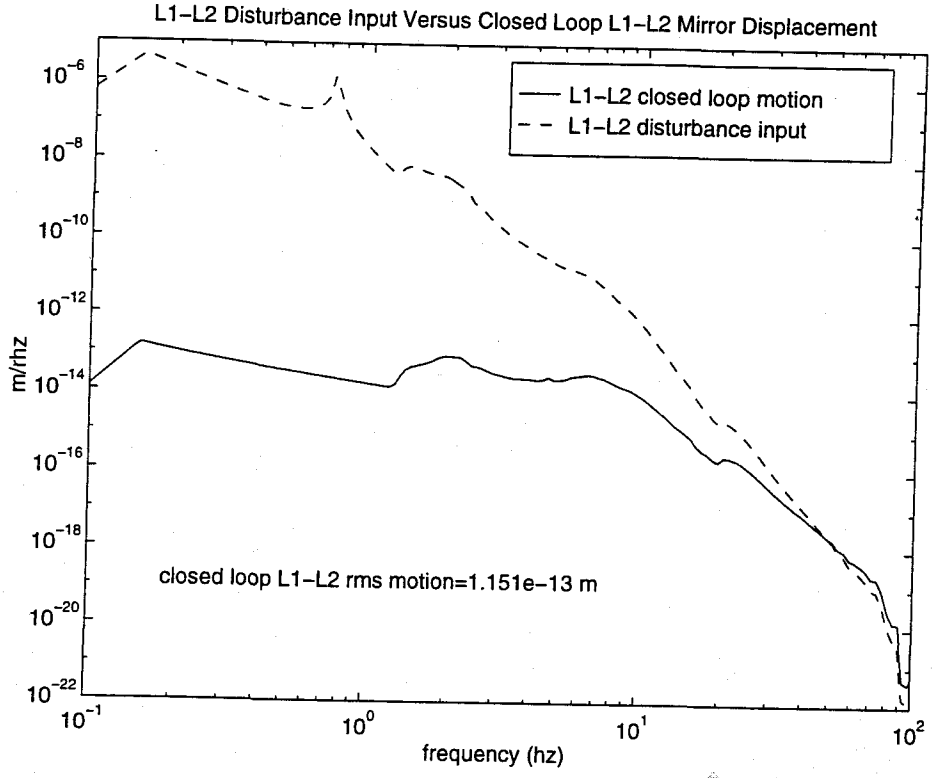

Figure 13: Open and Closed Loop RMS Motion for I- Loop.

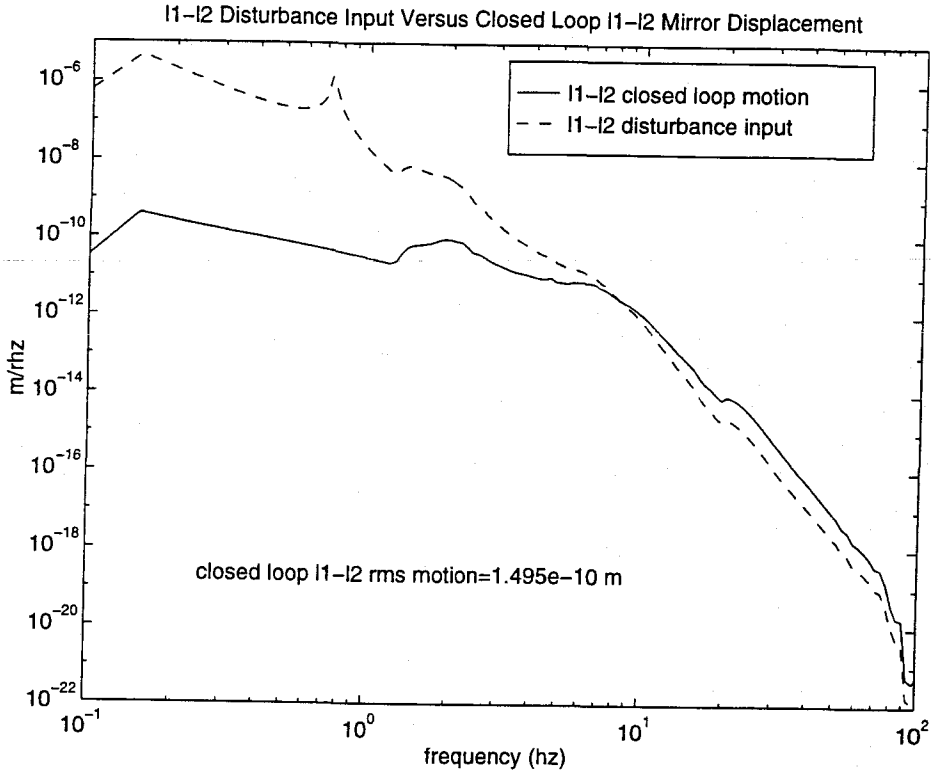

Figure 14: Cumulative RMS I- displacement (open- and closed-loop).

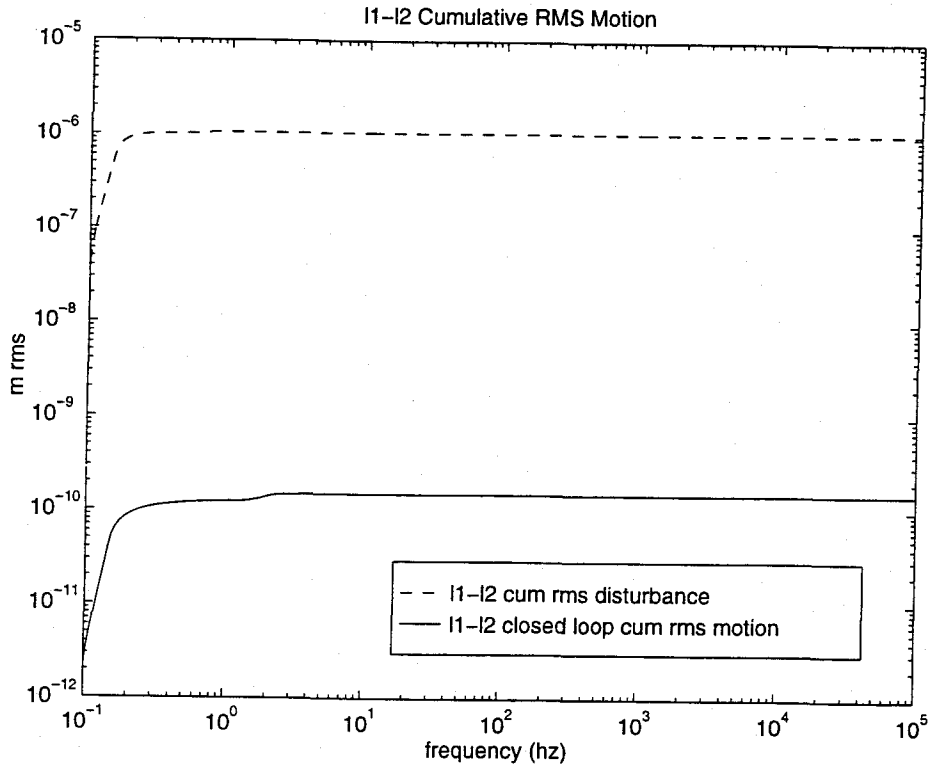

3.3.2. Results: Auxiliary Sensor Shot Noise

As detailed in the Science Requirements Document, shot noise in the L_- loop (sensor i_3) will dominate the interferometer readout noise spectral density above about 150 Hz (and also will contribute to the total noise at lower frequencies). However, the shot noise from any of the other sensors (controlling what are considered "auxiliary" degrees of freedom) may not contribute significantly to the expected noise; specifically, their shot noise may not degrade the net strain sensitivity by more than 0.5% per degree of freedom, and thus each individual contribution must lie at least 20 dB below the target SRD spectrum.

Calculation of the effect of shot noise in the main and auxiliary sensor signals started with an FFT analysis {REF?} of the power-recycled interferometer to determine the optical power on each photodetector. The FFT model used 1.06 micron wavelength light; the mirror surfaces assumed were scaled projections from the HDOS Calflat data with 1.6 nanometer RMS figure errors ('lambda/400' at 633 nm). Base losses of 50 ppm and mirror diameter of 30 cm were also assumed. The resulting equivalent photocurrents are given in Table 4.

The power levels were then used to calculate an equivalent shot noise current at the output of each demodulator. Using the small-signal optical response model ("Twiddle" {REF?}), these currents were converted into equivalent mirror displacements, as discussed in Appendix B. More details on the shot noise calculation can be obtained from "Shot Noise in the Length Error Signals" by P. Fritschel, LIGO-T960042.

Figure 15 shows the resulting shot noise contribution to the interferometer displacement sensitivity. Between 40 Hz and 140 Hz, the l_- shot noise in the sample design contributes an equivalent displacement spectral density 16 dB below the LIGO Science Requirement curve, somewhat exceeding the allowance.

This shortfall would be resolved by scaling back the overall l_- open-loop gain to bring the unity gain frequency from 22 Hz down to about 15 Hz. While such an adjustment would appear to further violate the closed-loop RMS residual motion requirement, recall that the microseismic noise was assumed to be uncorrelated for all mirrors. This is clearly an overly conservative assumption for l_-, since the vertex mirrors all lie within a small fraction of the 0.16 Hz microseismic wavelength. Based on long-term 40 meter interferometer differential arm displacement data (see Appendix A), we anticipate the actual microseismic input to l_- will be at least a factor of ten lower than assumed. In addition, it is worth noting that only relatively simple compensation has been used in the loop; increased margin can be achieved with modest filter enhancements.

Shot noise contributions of the i_1 and i_2 loops have not been treated here, since they would only arise through unmodeled imperfections in the optical common-mode rejection of the interferometer; however, they are expected to be considerably smaller in practice.

LIGO-T960027-01

Table 4: Photocurrent and shot noise current density at each sensor.

Demod output	*DC photocurrent* (mA)	*Shot noise* (A $Hz^{-1/2}$)
i_{s1}	33	1.02×10^{-10}
i_{s2}	0.05	3.97×10^{-12}
i_{s3}	276	2.97×10^{-10}
i_{s4}	20	8.09×10^{-11}

Figure 15: Shot noise contributions to displacement spectrum.

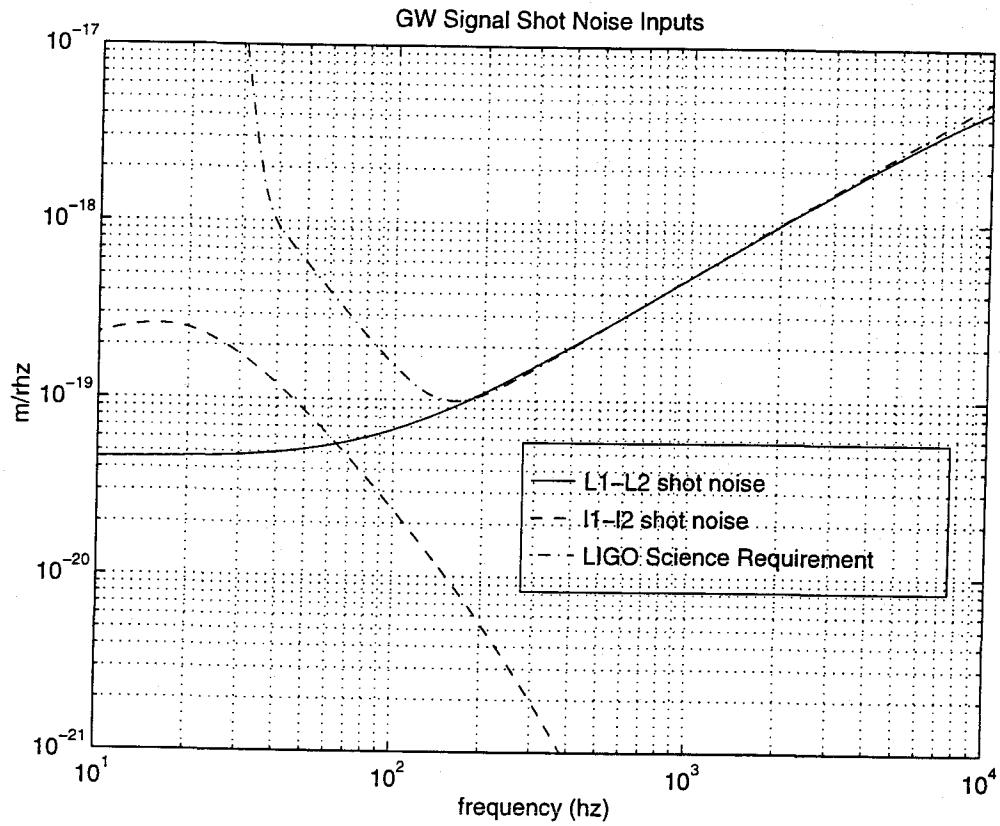

LIGO DRAFT

4. ACQUISITION MODE CONTROLS

The main requirement driving the Acquisition mode control design is the time it takes to acquire lock. To simplify the overall LSC design, the fundamental modulation topology for Acquisition mode is the same as for Detection mode. However, the requirements are significantly different, leading to different characteristics in the control compensation for each degree of freedom.

4.1. Loop Configuration

The servo topology looks very similar to the Detection mode configuration, with the addition of a nonlinear guided lock controller in the i_3 (L_1-L_2) loop, shown shaded in Figure 16.

Figure 16: Acquisition mode feedback configuration.

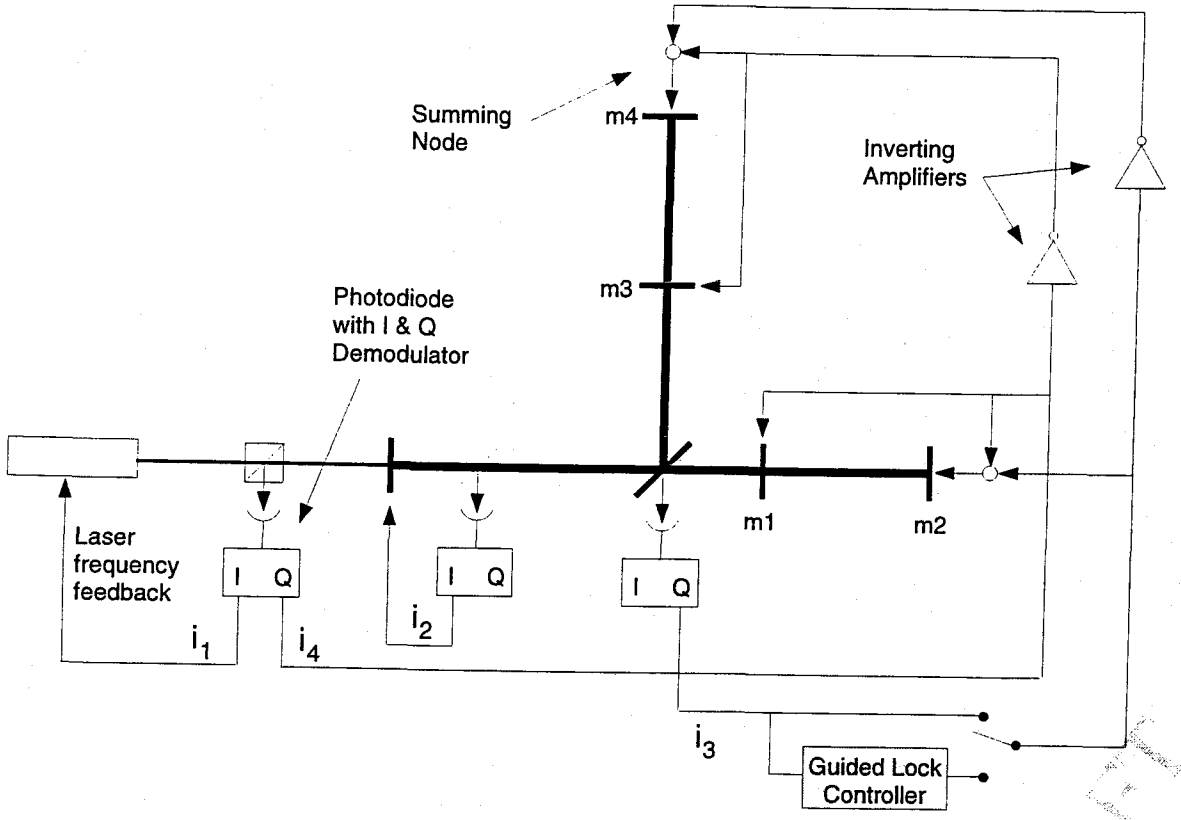

Modeling and simulation of the full power-recycled interferometer configuration have not advanced sufficiently to propose a concrete design at this stage. However, important guidance was derived from simulations of acquisition in a 3-mirror linear coupled cavity configuration. Some of the relevant findings are summarized below:

- The cavities lock in a natural sequence, whose ordering depends on the choice of signals being sensed.
- The ordering of the coupled cavity locking sequence was (1) sidebands resonate in the

recycling cavity first and then (2) carrier simultaneously resonates in the recycling cavity and arm cavity.

- For equivalent bandwidth servos, the threshold velocity of the arm cavity (maximum relative mirror velocity for capture) was significantly lower than that of the recycling cavity, mainly due to the narrower linewidth of the arm cavity

Several projections can made about locking a recycled interferometer based on the above observations:

- The Michelson degrees of freedom will have high threshold velocities, since the recycling cavity has low finesse.
- The common mode arm loop will also have a high threshold velocity since the bandwidth of the laser frequency correction servo will be high (i.e. at least 10 kHz).
- The differential mode arm cavity has narrow linewidth and its loop has low bandwidth, so it will most likely have a low threshold velocity. Preliminary estimates puts this threshold velocity as low as .1 micron/sec. Based on seismic estimates and current stack and suspension designs, an active guided lock controller would probably be needed to suppress mirror motion below this threshold reliably.

The current concept thus includes a nonlinear guided lock controller. Other differences from the Detection mode control system include:

- **Reallocation of gain & dynamic reserve.** Photodetector transimpedance, RF preamplifier gain, and possibly RF modulation index will be scaled back to increase the dynamic range of the front ends; complementary increases in the "back end" gain will be phased in. The transimpedance provided by SUS to drive the mirror coils may also be reduced, to increase the available peak force.
- **Reduced low frequency feedback.** High DC and low-frequency gain, needed in Detection mode to maintain low RMS errors, may interfere with dynamic reserve and complicate transient overload recovery. Modest gain will also help improve gain and phase margins.
- **Unconditional stability.** As the cavity circulating fields build, the optical gain rises from zero to its asymptotic value; the acquisition loops will need to be stable over a wide range of optical gains to maintain lock throughout the transient.
- **Increased bandwidth.** Threshold velocity has been shown to depend sensitively on control bandwidth. It may be beneficial to relax Detection mode bandwidth constraints. For example, the entire Acquisition transient is expected to last less than the equilibration time of test mass internal mode resonances, and the excess shot noise introduced by the I. loop (which constrains its gain) is not an issue for Acquisition.

4.2. Sequencing During Acquisition and Transition modes

During the acquisition process the LSC, ASC, and SUS are sequencing between different sensors, actuators, and controllers in order to complete the task of acquiring lock of the interferometer. In this particular mode the sequencing should be looked at from a systems perspective since the three

systems must function together in order for the interferometer to acquire (see Figure 4). The sequencing will be worked out in greater detail during the Preliminary Design phase.

LIGO-DRAFT

5. PHOTODETECTION SYSTEMS

The four independent interferometric degrees of freedom are derived from radiofrequency (RF) photocurrents detected by three photodetector units (each of which is demodulated at two independent RF phases). To meet the LIGO interferometer sensitivity goals while maintaining a practical implementation of other systems, these detectors must have a number of special capabilities:

- quantum efficiency > 0.8 at 1.06 micron wavelength
- no degradation in SNR up to 400 milliamperes^{TBR} of steady-state photocurrent
- high linearity and uniform RF response at this level of average photocurrent
- robustness against brief power transients (up to ~ watts^{TBR} for ~ milliseconds^{TBR})
- negligible electronic noise compared to the shot noise in detected photocurrent
- dynamic reserve adequate for acquisition and detection mode signal excursions
- high spatial uniformity in RF response (specifications TBD)
- compatibility with operating frequencies between 20 and 80 MHz (baseline: 37 MHz^{TBR})

LIGO will develop and engineer custom detector units, since units having these properties are not available commercially.

5.1. Photodetector Concept

Each photodetector unit includes:

- photodiode sensor(s)
- electronics to provide reverse diode bias
- electronics to filter and amplify the RF photocurrent for driving cables and balanced mixers
- electronics to read out the average (DC) photocurrent
- electronics to implement overload/overcurrent protection (as required)
- electronics to control gain and allocate dynamic reserve (as required)
- electronics to test and calibrate the unit
- a controllable incoherent light source for end-to-end LSC system shot noise tests

The optics needed to relay the sensed laser beam out of the vacuum system, match its diameter and shape to the photodiode active area(s), and divide the beam among multiple sensing elements (if required) are *not* included in this scope, although they must clearly be included in any design evaluation.

LIGO-T960027-01

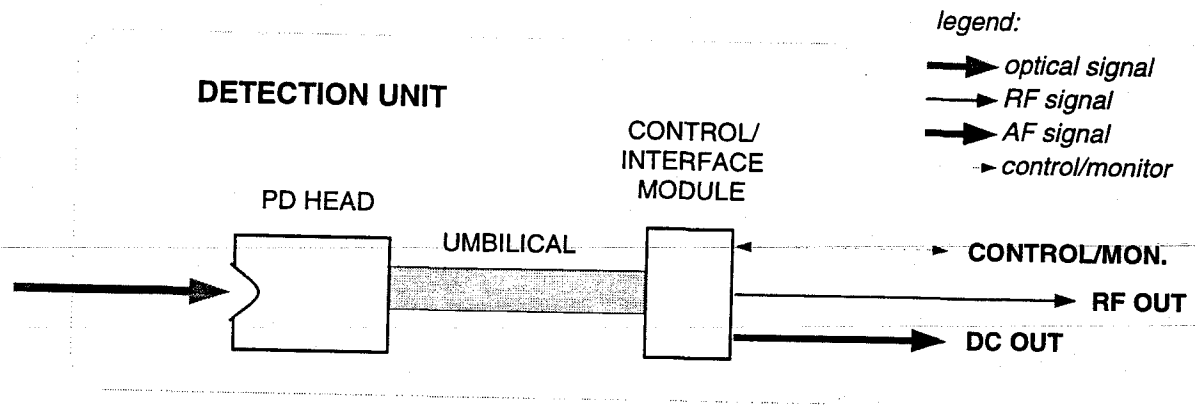

Figure 17: LIGO LSC photodetector unit block diagram.

Functions of each photodetector unit are distributed between a remote head, which will be located adjacent to LIGO Vacuum Equipment laser beam I/O ports in the Hanford and Louisiana Corner Station LVEA's, and a control and interface module located in a nearby electronic equipment rack. The control and interface module will be built in a 6U VME format or equivalent, while the detector head will have a custom RF-shielded housing. They will be joined by umbilical cable bundles (mixed 50 ohm coax and multiconductor in a common shield) about 10 meters[TBR] in length. For a view of how the detectors fit within the scope of the LIGO LSC system, refer to Figure 3.

5.1.1. Diode selection

To date, silicon PIN photodiodes have been used LIGO interferometer prototypes operating with the 515 nm Argon ion laser line. However, even IR-enhanced silicon devices have relatively poor quantum efficiencies (of order 50%) at 1060 nm. Also, space charge saturation, power dissipation and damage effects appear to limit their tolerable photocurrent density to 20 mA/cm^2 or less. Standard "large area" Si PIN diodes like those used in LIGO prototypes (for example, the EG&G SGD-444 and DT-110) could thus each take about 1/20 the required steady-state flux. The optical and electronic implications of dividing the beam power among as many as 20 individual diodes are formidable, and the resulting implementation would be undesirably complex, cumbersome and costly.

As a result we are reluctant to use silicon. At the moment the best alternative appears to be InGaAs, which promises significantly greater quantum efficiency (85% or better) and much higher current density per unit area (1 A/cm^2 has been advertised). While these are obviously attractive features, at least two difficulties need to be addressed:

- Production and characterization of devices in this material have not advanced to the same maturity as for silicon. In particular, large-area (> 3 mm diameter) devices are only recently becoming available.
- LIGO has no experience using these devices in sensitive interferometers. For example, detecting the weak RF signal photocurrent in the presence of large noise currents at other frequen-

cies and modal interference through spatial nonuniformities in the quantum efficiency present significant concerns.

We hope to address some of these concerns during the LSC preliminary design phase by testing prototype detector devices and systems, as discussed below.

5.1.2. Head layout concept

Although the optical design of the matching and dividing optics formally lies outside the LSC scope of work, it must be considered an intimate part of the head configuration. Among other things, the external optics must accommodate:

- number of physical diodes
- angle of incidence on each diode (and anamorphic imaging if angle is large)
- diode diameter and allowable peak power density
- equal optical path (tolerance TBD) to each diode element from interferometer optics
- minimization of backscatter
- TV monitoring of spatial intensity distribution

These factors are highly dependent on the precise choice of photodiode, and therefore early work to choose a baseline device has high priority. In addition, the head's remote location and critical SNR subjects it to significant RFI, ground loop and antenna problems which must be accommodated by careful package design. A schematic package concept addressing some of these concerns is depicted in Figure 18. Some features worth noting:

- Matching & dividing optics and CCD fringe monitor camera, while formally outside the LSC work scope, must be designed in conjunction with head.
- A subdivided enclosure provides isolation of sensitive RF components from other circuitry.
- Stepped detector placement is intended to maintain identical optical path from interferometer to each detector surface. This simplifies beam imaging and mitigates potential scattering noise.
- Possible angled placement of diodes (to improve quantum efficiency and reduce backscatter) and associated anamorphic imaging components are not shown explicitly.
- An electromechanical shutter, required for "dark" testing and possibly as one component of the detector overload protection, is not shown; it would probably be located just below the modematching telescope.

LIGO-DRAFT

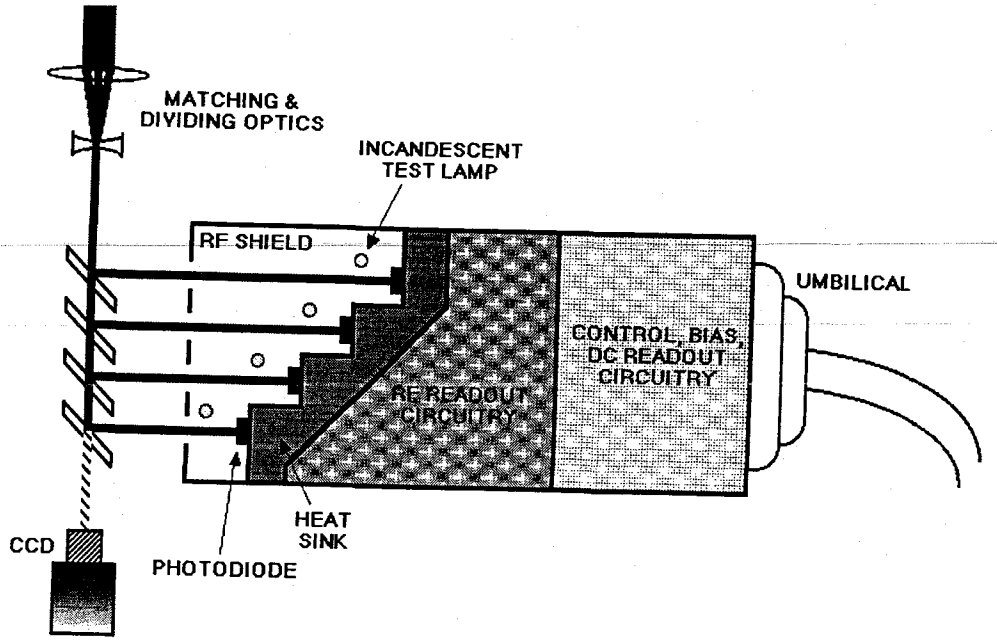

Figure 18: *Photodetector head layout concept* (four diodes shown, actual number TBD).

5.1.3. Electronics concept

Radiofrequency photodetector circuits used in LIGO prototypes have typically been of the form depicted in Figure 3. An inductor is tuned to resonate with the diode junction capacitance[1] at the working frequency. A low-noise preamplifier (with noise impedance matching the resonant impedance of the diode tank circuit) drives the 50Ω double-balanced mixer. The effective shunt resistance of the diode itself (Figure 4) is a critical parameter in the system SNR and dynamic reserve; this may vary significantly between devices of the same nominal type. This effective shunt is generally much lower and less controlled than the DC leakage impedance usually specified by the manufacturer, and may depend on operating frequency.

Frequently the dynamic reserve of the system as a whole is constrained by the maximum signal level accepted by the mixer. As a result high preamplifier gain is not generally admissible (at least for lock acquisition, where there are large RF transient signals). Detectors in the 40 meter prototype have had voltage gain $\mathbf{A_{RF}} \sim 1$ and LC circuit effective impedances of 0.5 -2 kΩ at resonant operating frequencies around 10 MHz.

1. of order 100 pF for typical 1 cm^2 Si PIN diodes reverse-biased at 150 volts

LIGO-DRAFT

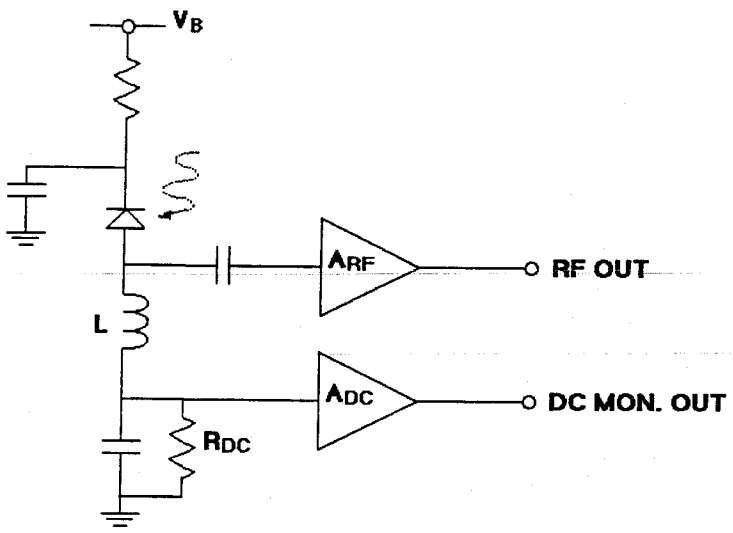

Figure 19: Conceptual schematic of individual photodiode readout circuit. Inductance L is chosen to resonate with junction capacitance of photodiode at working frequency. Not shown are additional bandpass filters and notch traps for harmonics of the modulation frequency, usually included in the RF amplification stage.

LIGO will use higher operating frequencies (around 40 MHz), and InGaAs diodes will generally have higher C and lower effective shunt impedance per unit area (at admissible reverse bias voltages). Although they may have less total capacitance per unit *power* accepted, it may be still more difficult to match these detectors to available preamplifiers. Nonetheless, at the higher photocurrent levels envisioned, simple broadband transimpedance stages (e.g. just a load resistance and preamplifier) may be appropriate.

The diode electrical parameters will also determine the optimal way to combine diode outputs. Electrical addition of RF preamp outputs from individual circuits like that shown in Figure 3 would be the most straightforward implementation, but impedance matching and SNR considerations may require photocurrent addition prior to active stages (e.g. using transformers to achieve the equivalent of a "series" connection, to increase the effective noise impedance).

LIGO DRAFT

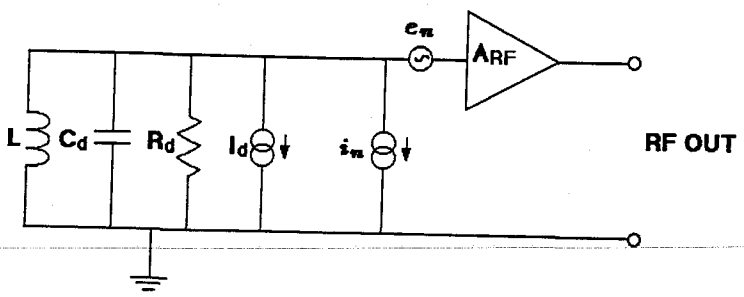

Figure 20: Radiofrequency equivalent circuit. Effective photodiode junction capacitance C_d and shunt resistance R_d may depend on photocurrent I_d, leading to intermodulation. e_n and i_n are voltage and current noise of RF preamplifier, respectively.

5.1.4. Overload protection

The stored circulating power inside the recycling cavity of an operating LIGO interferometer will be over 100 W. Loss of length control during operation will momentarily permit some of this power to appear at the dark (antisymmetric) port, temporarily subjecting the photodetectors to severe overload conditions. The amplitudes, durations and waveforms of these power transients depend on the detailed optical and mechanical behavior of the interferometer; numerical modeling of these transients is a high priority for the preliminary design phase. In any case it is evident that a combination of robust design and explicit protection mechanisms will be necessary.

Electromechanical shuttering may be too slow to afford adequate transient protection, and electrooptic or acoustooptic shutters will introduce undesirable optical losses, limiting the effective quantum efficiency. Each of these will also be cumbersome and costly to engineer. It is hoped that instead a combination of robust device selection, conservative thermal design and fast-acting electrical protection can prevent damage.

This electrical protection may take the form of a fast crowbar on the detector's reverse bias. In the reverse-biased condition (required for bandwidth and linearity in operation) an InGaAs junction may dissipate an order of magnitude more heat than with bias removed. As a result it is important to establish not only the damage threshold and overload withstand time under biased, operating conditions, but also with the bias removed (or reduced) to simulate such a "protection" mode.

5.2. Open Issues and Test Program Targets

As indicated, strategic testing is needed both to validate expected performance models and to enable optical and electronic preliminary designs. Four phases of testing are envisioned:

1. InGaAs feasibility studies, selection of candidate manufacturers and devices
2. Preliminary tests on candidate devices:
   - power handling/damage threshold (biased & unbiased)
   - linearity & RF gain compression vs. DC power

LIGO-T960027-01

3. Refined device tests:
   - RF intermodulation vs. DC power
   - spatial uniformity (RF and audio)
4. Integrated prototype testing on LIGO PNI facility

The preliminary tests (phase 2 above) will be designed to focus on early determination of critical parameters strongly affecting the matching and forming optics and the electronics design activities. For example, it is anticipated that diode number, diameter, and angle of incidence will be provisionally adopted at the end of this phase, as will current per diode, bias voltage and protection requirements.

The third testing phase would proceed in parallel with electronic and optical design, to determine parameters related to noise processes. In general these explorations are expected to have less impact on system optimization (though significant findings may still have design repercussions). They are expected to illuminate interactions with scattered light, spatial mode quality and laser amplitude noise. A conceptual schematic of a test setup suitable for preliminary and refined tests of this nature is shown in Figure 21.

Finally, we plan to perform integrated testing of an advanced detector prototype on the LIGO PNI (Phase Noise Interferometer) facility during and after its conversion to 1.06 micron wavelength operation. These tests will explore noise processes in detail, and permit operational verification of basic operation and SNR characteristics.

LIGO-DRAFT

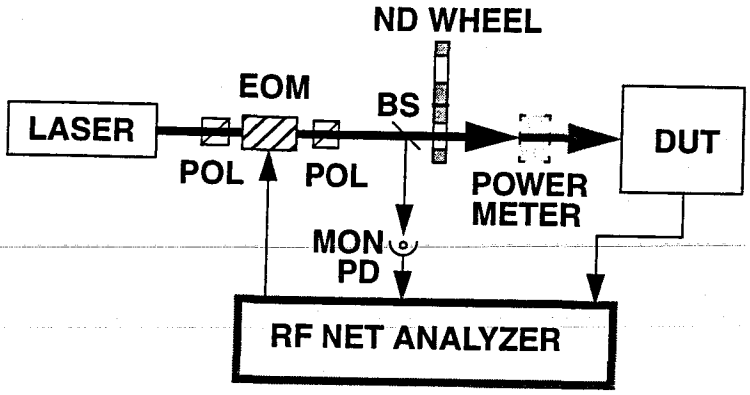

Figure 21: Schematic of photodiode/photodetector unit testing setup. Light from diode-pumped 1060 nm solid state laser (500 mW class) is amplitude modulated by an electrooptic modulator (EOM) between crossed polarizers (POL). The diode under test (DUT) may be mounted on XY translation mounts to investigate spatial nonuniformity. Not shown are lenses to achieve the desired beam profile at the diode surface, and a beam scanning instrument needed to establish and periodically verify this profile. Neutral density (ND) filters just ahead of the DUT permit variation of power without affecting laser or EOM spatial and temporal characteristics.

LIGO-DRAFT

6. CALIBRATION

The interferometer strain readout voltage will be related to astrophysical strain through a fairly complex response function, which depends on numerous parameters. Some of these parameters can be measured independently and are expected to be stable over time; however, at the high relative accuracy required, many multiplicative parameters are expected to fluctuate by fractional amounts comparable to the entire error budget.

These variations will in general alter both the calibration level and the frequency response. As a result, frequency response calibration measurements will be taken periodically (interval TBD pending settlement of allowable tolerance). To "anchor" the frequency response measurements, a continuous sinusoidal test signal or signals may also be required in Detection mode; depending on the variability of the transfer function shape, several test signals may be applied at different frequencies.

Precise methods for establishing the initial calibration and maintaining it throughout operations will be developed during the preliminary design phase. One model for this sequence can be taken from operation of the 40 meter interferometer;

- **Initial calibration of intermediate standard:** The force/current characteristics of one or more core optics suspension actuator subsystems will be established, probably by several independent means. These may include:
  - Direct measurement of the net magnetic dipole moment of each magnet attached to the core optic, the mass of the optic, and the inductance and position of each SUS actuator coil before installation
  - *In situ* measurement of the displacement of the CO mirror vs. SUS actuator coil current using a low-power auxiliary Michelson interferometer with fringe interpolation
  - *In situ* measurement of the displacement of the CO mirror vs. coil current by driving the mirror through a full free-spectral range at low frequency
- **Measurement of SUS coil current vs. injected test signal voltage:** The calibration test signal injection will pass through some electronics before appearing as a coil current; the coefficient (which will generally be frequency dependent) will have to be established and periodically verified.
- **Frequency response calibration:** With a known sinusoidal test signals injected at a series of frequencies, the readout is monitored to determine the ratio between DAQ input voltage and injection test voltage. This is combined in software with the initial intermediate standard and test signal calibrations to determine the readout voltage as a function of displacement (or force).
- **Continous monitoring and update:** The frequency response calibration will be a sensitive function of the L_- control loop gain. Variations in mirror alignment, input power, and other parameters over time and temperature will modify the loop gain, and may cause excessive calibration errors in the interval between frequency response measurements (which cannot be too frequent, since they are perturbative and cause loss of data). In this case, small-amplitude sinusoidal test signals may be injected continuously at several frequencies to allow a running update of the frequency response without degrading sensitivity. These test signals can be removed by filtration during data analysis, after they are used to update the local calibration in each frequency band.

- **Check, doublecheck, check again:** New calibration errors or variations in assumed "stable" parameters are likely to occur over time. Initial standard calibration and intermediate steps will be repeated periodically such that, if changes do occur, the affected period of suspect data will be minimized and (if feasible) data can be recovered by localization of the fault. In addition, independent cross-checks of calibration using different physical mechanisms will be employed to validate fundamental assumptions about the calibration chain and standards. These checks can also serve to bridge large extrapolations in test signal magnitude, arising, for example, from the disparity (twelve orders of magnitude) between the LIGO target displacement sensitivity and the most convenient absolute standard, the laser wavelength. Several such independent methods have either been proven at relevant precision or show promise:
  - *Residual gas index fluctuation noise.* Gas noise depends only on pressure, temperature and gas composition; there are no other free or measured parameters. Admitting a non-condensible test gas to the beam tubes with the ion pumps temporarily sealed should provide a relatively straightforward and fundamental calibration check. On the 40 meter interferometer this type of measurement was readily capable of 5% absolute accuracy.
  - *Comparison of shot noise with direct model calculation.* Although the shot noise depends on a fair number of optical parameters, many of them can be measured by several redundant means, giving the potential for high credibility and accuracy. Addition of pure incoherent shot noise (from incandescent test lamps), variation of laser power, and variation of the RF modulation index allow further validation of model inputs. Exact accuracy depends on the quality of these ancillary measurements, but in any case should be better than 10%.
  - *Photon recoil.* Measurement of the test mass recoil due to reflection of flashlamp or laser pulses or a modulated CW laser beam can provide independent calibration as accurate as the measurement of the light source power, probably better than 10%.
  - *Gravity gradients.* It should be feasible to construct a spinning quadrupole rotor which couples tidally to a nearby test mass with sufficient strength to make a reliable measurement. It is not yet clear what accuracy one might achieve, and numerous systematic confounds may interfere (like vibration or electrical crosstalk), but at some level it would be aesthetically very elegant to calibrate LIGO gravitationally.

LIGO-DRAFT

A. SEISMIC EXCITATION MODEL

Figure 22 shows a straight-line fit to ground displacement data taken at the Livingston site, Washington site, and the 40 m lab during noisy conditions. The open loop test mass motion for the different sites can be calculated by filtering a given ground noise spectrum through the 4 layer Viton[1] stack (i.e. horizontal to horizontal transfer function) referenced in LIGO-T952005, and a 0.74 Hz pendulum with a Q of 10^6 (see LIGO-T950011-06-D). The resulting power spectral density for the motion of a test mass at each of the three sites is shown in Figure 23. The Livingston Parish data were used for the analysis in this report since they stress the control design the most.

Figure 22: Seismic displacement spectrum (approximation).

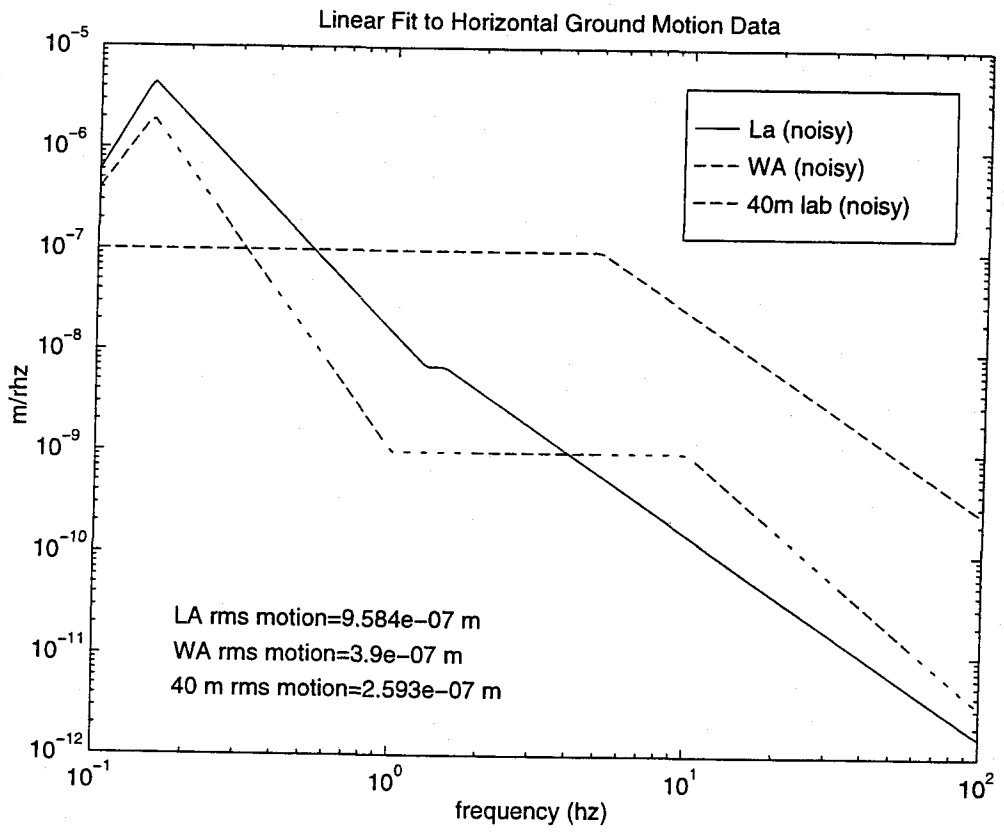

1. Tradename (flouroelastomer).

LIGO-DRAFT

Figure 23: Estimated net TM motion (open-loop).

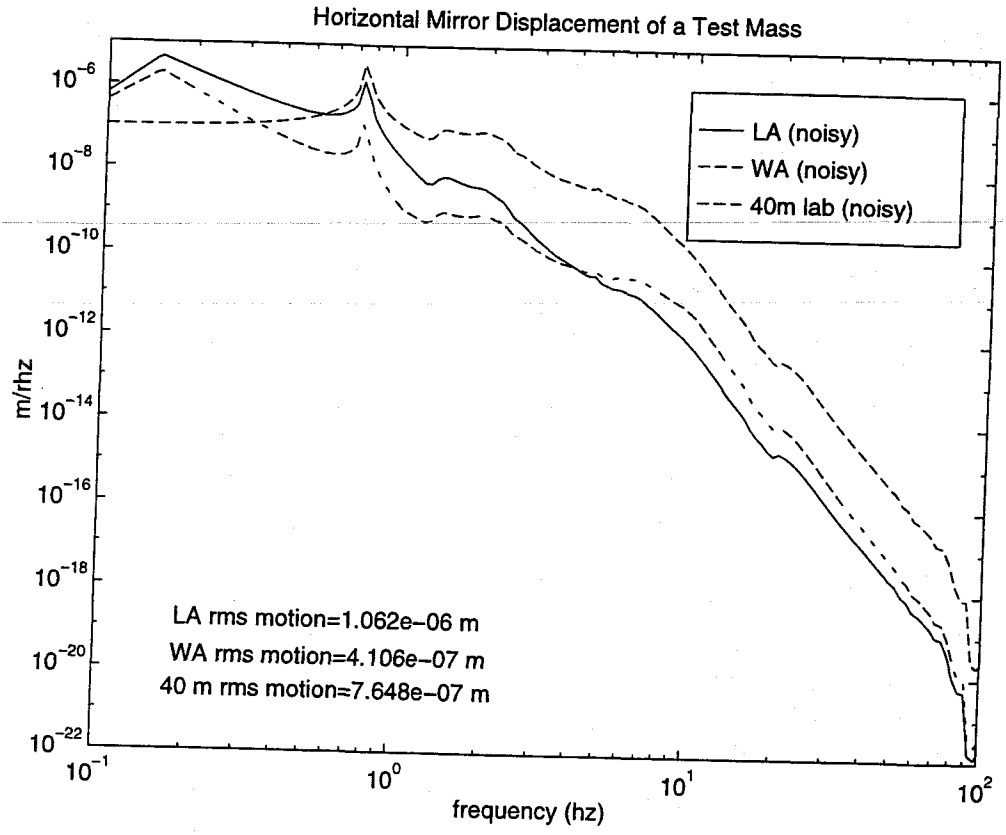

LIGO-DRAFT

B. SHOT NOISE MODEL

In order to do the shot noise calculation, the interferometer control system dynamics were written in matrix notation. The following notation was used:

$$ii(s) = \begin{bmatrix} i_{s1} \\ i_{s2} \\ i_{s3} \\ i_{s4} \end{bmatrix} = \text{equivalent demodulator current shot noise}$$

$$dl(s) = \begin{bmatrix} Phi \\ l_1 + l_2 \\ L_1 - L_2 \\ l_1 - l_2 \end{bmatrix} = \text{length and phase disturbance inputs}$$

$P_1(s)$ = 4x4 plant transfer function matrix from $dl(s)$ to $i(s)$

C(s) = 4x4 controller transfer function matrix from $i(s)$ to $dl(s)$ (off-diagonal elements=0)

$P_2(s)$ = gravity wave readout filter = the (1,1) component of $\{[C(s)P_1(s)]^{-1}\ [I+C(s)P_1(s)]\}$

$gw(s)$ = calibrated gravity wave readout signal

s = Laplace variable ($\sigma+i\omega$)

Figure 24: Block Diagram of Interferometer Control System

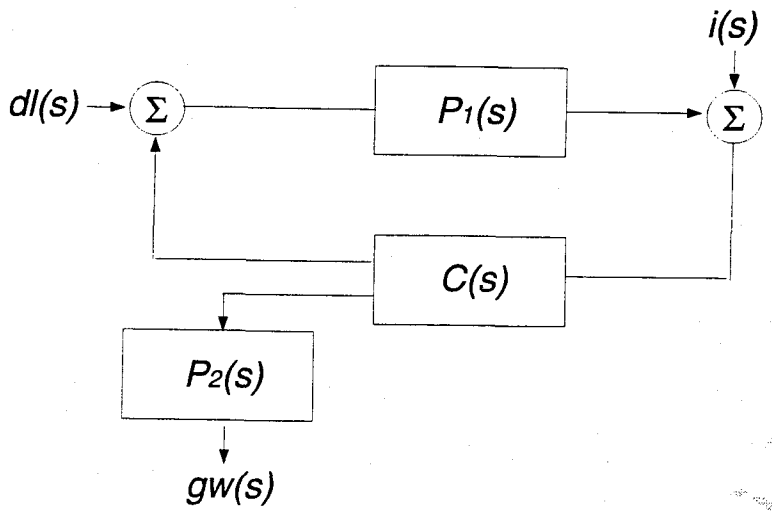

The block diagram for the interferometer control system is shown in Figure 19. An expression for the shot noise contribution of each sensor to the gravity wave readout signal can be derived using the block diagram and matrix algebra manipulation. The resulting expression for the gravity wave

readout signal as a function of demodulator shot noise current from each of the sensors is listed below.

$$gw(s) = P_2(s)[I + C(s)P_1(s)]^{-1}C(s)i(s)$$

The adopted method in LIGO for calculating the plant transfer function, $P_1(s)$, is to use the program Twiddle. It is very important to use the correct units when calculating the equivalent shot noise current at the demodulator output in order to interface properly with the Twiddle calculation. Below is a list of Twiddle assumptions that will effect the units.

1. Twiddle assumes a total input power of 1 Watt (i.e. carrier plus sideband power) into the interferometer.
2. In Twiddle the plant transfer function $P_1(s)$ is in units of (i/λ) where the current i, is the current in amps at the output of the demodulator and λ is the wavelength of the carrier.
3. Twiddle assumes a photodetector efficiency η = (.8 electrons/photon) = (1 amp/watt).
4. The inphase demodulation is calculated using the following equation where i_p is the photodetector current.

$$i(t) = \frac{\omega_m}{2\pi} \int_t^{t+\frac{2\pi}{\omega_m}} i_p(t')\cos(\omega_m t')dt'$$

   (for quadphase demodulation, the integral contains $sin(\omega_m t')$).
5. The transfer functions are generated assuming a unit of motion for each of the mirrors being actuated (i.e. if you shake m_1+m_2, both m_1 and m_2 are each moving a unit of motion equal to Δx).

LIGO-DRAFT

C. ELECTRONIC GAIN: L_ LOOP EXAMPLE

The loop gains calculated in Section 3. are each a product of an optomechanical transfer function, which is largely predetermined by top-level requirements (power, storage time, pendulum isolation factor, etc.), and an electronic compensation transfer function, which has to be subjected to realistic engineering. It is thus instructive to bound this electronic transfer function by numerically evaluating the optomechanical part.

Consider the L_ loop (Figure 6). A simplified picture showing the optical and electronic components of the transfer function for this loop alone is shown below.

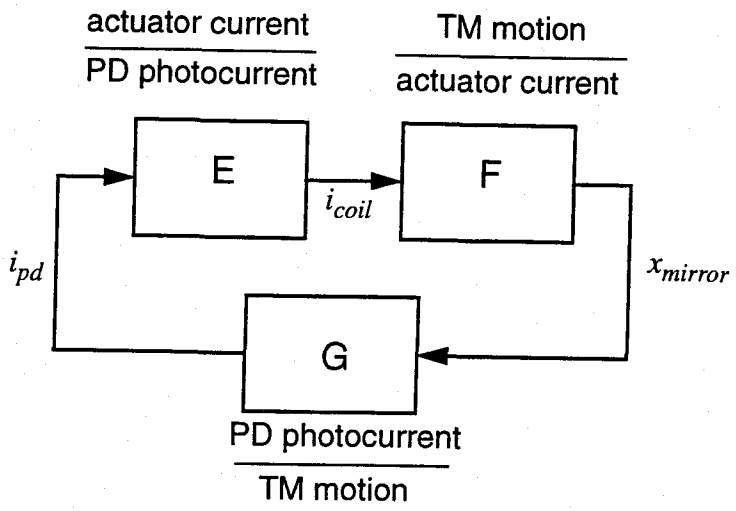

Figure 25: Simplified diagram of L_ loop.

Here E is the transfer function of the electronics, from RF photocurrent to coil actuator current; F is the amount of test mass displacement (in meters) per unit actuator current (in amperes); and G is the expected RF photocurrent per unit test mass displacement.

From Section 3., Appendix B and LIGO-T950011-06-D ("Suspension DRD"), we have

$$G \equiv i_{pd}/x_{mirror} \approx 5.7 \times 10^{9} \text{ A/m} \times \left[1 + \left(\frac{f}{f_c}\right)^2\right]^{-1/2}$$

and

$$F \equiv x_{mirror}/i_{coil} \approx 9 \times 10^{-5} \text{ m/A} \times \left[1 + \left(\frac{f}{f_s}\right)^2\right]^{-1}$$

where $f_c \approx 90$ Hz is the arm cavity pole frequency and $f_s \approx 0.75$ Hz is the pendulum frequency of the suspension.

Thus to implement the loop gain characteristic shown in Figure 9 (about $3 * 10^6$ at 1 Hz, and unity at 140 Hz) the magnitude of the electronic gain E must be about 17 A/A at 1 Hz and 0.13 A/A at 140 Hz. The transimpedance supplied by SUS for force actuation will be approximately 1 kΩ; current thinking is that the photodetector transimpedance will be about 100 Ω. Thus the forward

voltage gain of the Detection mode L_- loop controller will have to be about 170 at 1 Hz and about 1.3 at 140 Hz.

This relatively low voltage gain within the signal band will present considerable challenges in the realization of the electronics. Effectively, it implies that the noise tolerance at the "output" is identical to that at the photodiode; that is to say, sensitivity to electronic pickup, Johnson noise, amplifier noise etc., which are usually relaxed in the final stages of the servo amplifiers by the gain of preceding stages, are equally critical everywhere. Furthermore, analog implementation of transfer functions having low-frequency poles and zeros (using RC networks) is technically very difficult if voltage noise constraints force the use of very low impedances. Scaling up the output transimpedance (or reducing the photodetector transimpedance) would appear to help, but the dynamic range and SNR of the controller (along with practical power supply voltages) sharply limit this flexibility.

Practical electronic realization of the required transfer functions will be a top priority during the preliminary design phase.

LIGO-DRAFT

D. ALTERNATE READOUT OPTIONS

D.1. Frequency-shifted subcarrier

{to be added: summary of FSSC scheme}

D.2. Additional nonresonant phase modulation

{to be added: summary of second modulation scheme, ASC need, and LSC application}

LIGO-DRAFT

E. ACRONYMS & DEFINITIONS

The following acronyms and special terms are used throughout this document and some of its references. Unresolved or ambiguous terminology should be reported to the authors and to the Systems Engineering and Integration group for resolution.

- PSL - Prestabilized Laser
- IOO - Input / Output Optics
- COC - Core Optics Components
- ASC - Alignment Sensing and Control
- LSC - Length Sensing and Control
- SUS - Suspension Control
- SEI - Seismic Isolation
- CDS - Control and Data Systems
- SYS - Detector Systems Engineering
- IFO - LIGO interferometer
- SRD - LIGO Science Requirements Document
- DAQ - Data Acquisition System
- SNR - Signal to Noise Ratio
- AF - Audio Frequency
- RF - Radio Frequency
- IF - Intermediate Frequency

LIGO-DRAFT

F. APPLICABLE DOCUMENTS

F.1. LIGO Documents

Title	*DCC Number*
LIGO Science Requirements Document	LIGO-E950018-00-E
Detector Systems DRD	LIGO-T950065-00-D
LSC Design Requirements Document	LIGO-T960058-00-I
Frequency, Intensity and Oscillator Noise in the LIGO	LIGO-T960019-00-D
Shot noise in the Length Error Signals	LIGO-T960042-00-D
Prestabilized Laser DRD (B DCC)	LIGO-T950030-03-D
Core Optics Components DRD	LIGO-E950099-01-D
Ph. D. Dissertation, M. Regehr	LIGO-P940002-00-I
40-Meter Reference Source System Specification	LIGO-XX_TBD_XX
Suspension DRD	LIGO-T950011-06-D
LIGO Length Sensing System: Design Considerations...	LIGO-T952109-01-I
CDS Online Diagnostic and Readout Functions	LIGO-T960031-00-E
ISC Inter-Station Signal Transmission	LIGO-T960057-00-I
Concept for LSC Design During Detection Mode	LIGO-T960032-03-I
LSC Photodetector Development	LIGO-T960038-00-I
ASC Design Requirements Document	LIGO-T952007-00-I

Table 5: Applicable LIGO Documents

LIGO-DRAFT

F.2. Non-LIGO Documents

1. *VIRGO Final Design v. 0.* The VIRGO Collaboration (6/95)
2. *Diodes selection, the first approach.* VIRGO internal report PJT94-014, by A. Dominjon and M. Yvert (5/94).
3. Ultrahigh-frequency stabilization of a diode-pumped Nd:YAG laser with a high-power-acceptance photodetector. N. Uehara and K. Ueda, **Opt. Lett. 19** (10), p. 728 (1994).
4. *1995 Emitters and Detectors catalog*. EG&G Optoelectronics Canada (1995).
5. *InGaAs-PIN Photodiodes*. Data sheet # KIRD 1002E03, Hamamatsu Corporation (1993).
6. Guided lock acquisition in a suspended Fabry-Perot cavity.J. Camp, L. Sievers, R. Bork and J. Heefner, **Opt. Lett. 20** (24), p.2463 (1995).
7. Drawing **V049-5-001,** *Equipment Arrangement Plan, Corner Station Washington, LIGO Vacuum Equipment.* Process Systems International (3/96) (LIGO DCN is TBD).

LIGO-DRAFT